NeuroImage 333 (2026) 121942

Contents lists available at ScienceDirect

NeuroImage

journal homepage: www.elsevier.com/locate/ynimg

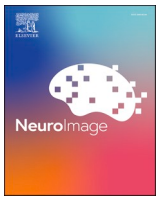

Frequency-specific prefrontal inter-brain synchrony and reinforcement learning signatures differentiate cooperative and competitive risky decision-making: An fNIRS hyperscanning study

Mingjing Wang [a,b], Sihua Xu [a,b,*], Linden J. Ball [c]

[a] Center for Magnetic Resonance Imaging Research & Key Laboratory of Brain-Machine Intelligence for Information Behavior (Ministry of Education and Shanghai), Shanghai International Studies University, Shanghai, China
[b] School of Business and Management, Shanghai International Studies University, Shanghai, China
[c] Human Factors Laboratory, School of Engineering and Computing, University of Lancashire, Lancashire, UK

ARTICLE INFO

Keywords:
Decision-making
Cooperation
Competition
Computational modeling
fNIRS
Hyperscanning

ABSTRACT

The neural and computational mechanisms that distinguish cooperative from competitive strategies in risky decision-making remain incompletely understood. In this study, we combine frequency-specific prefrontal inter-brain synchrony (IBS) measured via functional near-infrared spectroscopy (fNIRS) hyperscanning with reinforcement learning modeling to examine how social context shapes dyadic choice. Sixty female dyads performed cooperative or competitive variants of a modified Iowa Gambling Task (IGT). Behaviorally, competitive pairs achieved significantly higher cumulative earnings than cooperative pairs. Reinforcement learning analyses indicated that the Outcome Representation Learning (ORL) model provided the best account of behavior. Cooperative dyads showed increased sensitivity to win frequency (β_{fre}), suggesting a tendency to favor frequent but suboptimal gains. In contrast, competitive dyads adopted more flexible strategies that were less dependent on reward frequency. Neuroimaging results revealed dissociable frequency related patterns. Ultra-low frequency coupling in the dorsolateral prefrontal cortex (DLPFC) within the range of 0.015 to 0.017 Hz was associated with goal directed control and higher earnings. Higher frequency coupling in the frontopolar cortex (FPC) within the range of 0.340 to 0.381 Hz was associated with opponent monitoring and sustained competitive engagement, and was reduced during cooperation, consistent with reduced individual responsibility. These findings support a dual pathway account in which competition engages both control and monitoring processes to facilitate performance, whereas cooperation may incur performance costs through socially shaped learning biases. The results provide mechanistic insight into social decision making and identify candidate neural markers for adaptive behavior in interactive contexts.

1. Introduction

Risky decision-making has been extensively studied at the individual level, providing a robust theoretical foundation for understanding behavior under uncertainty (Arnold et al., 2025; Nejati et al., 2024; Reale, 2023; Viscusi et al., 2011). However, many real-world decisions occur in social contexts, where cooperation and competition fundamentally shape outcomes, requiring continuous mutual adaptation and additional cognitive processes such as monitoring others' intentions and integrating shared goals (FeldmanHall and Shenhav, 2019; Huang et al., 2025; Lockwood et al., 2018; Roos et al., 2024; Ruff and Fehr, 2014; van Baar et al., 2021). To capture these complex dynamics, researchers increasingly combine social neuroscience with computational modeling, linking neural activity to reinforcement learning (RL) processes (Frith and Frith, 2012; Suzuki and O'Doherty, 2020). In particular, frequency-specific prefrontal inter-brain synchrony (IBS) provides a neural marker of real-time social coordination (Cui et al., 2012; Reindl et al., 2018), and connecting it to RL-derived latent variables enables mechanistic insights into how interacting brains encode prediction errors, update values, and guide adaptive behavior. For example, fMRI studies show that the lateral prefrontal and frontopolar cortices arbitrate between model-based and model-free predictions, modulating behavior

* Corresponding author: Center for Magnetic Resonance Imaging Research & Key Laboratory of Brain-Machine Intelligence for Information Behavior (Ministry of Education and Shanghai), Shanghai International Studies University, 550, Dalian West Street, Shanghai, 200083, China.
E-mail address: xusihua80@gmail.com (S. Xu).

https://doi.org/10.1016/j.neuroimage.2026.121942
Received 12 October 2025; Received in revised form 28 March 2026; Accepted 20 April 2026
Available online 20 April 2026

via top-down control, while rostral anterior cingulate activity tracks cue-related expected value (Jones, 2011; Wan Lee et al., 2014). Those syntheses enable a shift from descriptive behavioral comparisons to a process-level understanding of how neural coupling supports strategic adaptation under cooperative and competitive conditions. Nevertheless, despite growing advances in behavioral and neuroimaging research, the neural mechanisms and computational processes that differentiate cooperation from competition in risky decision-making remain insufficiently understood (Wang et al., 2018).

Prior studies have primarily contrasted cooperation and competition as two dominant patterns of social interaction. Cooperation can boost group performance through resource sharing and complementary expertise (Stolle et al., 2024; Takada et al., 2023) but may also trigger free-riding and responsibility diffusion, reducing efficiency (Cooper, 2024; Darley and Latane, 1968). Competition, conversely, can enhance the subjective value of gains via reward-related processing (Gärling et al., 2020; To et al., 2018), yet may also promote risk-seeking. RL-modeling studies further reveal that prior cooperative or competitive experiences shape subsequent decisions in strategic games (Schulze and Newell, 2015; Vlaev and Chater, 2006). These models—including Expected Value (EV), Prospective Valence Learning (PVL), Win-Stay-Lose-Shift (WSLS), Outcome Representation Learning (ORL), Value-Plus-Persistence (VPP), and Value and Sequential Exploration (VSE)—provide a principled framework for estimating cognitive parameters such as reward sensitivity, choice persistence, and learning rates (Junyi et al., 2023; Kumar et al., 2019; Steingroever et al., 2018; Worthy and Maddox, 2014). Yet, most RL-based investigations focus on individuals, leaving the computational basis of joint decision-making largely uncharted.

Neuroimaging studies using fMRI and functional near-infrared spectroscopy (fNIRS) have consistently identified prefrontal regions as key hubs in social and value-based decision-making (Fareri and Delgado, 2014; Fliessbach et al., 2007). In particular, the prefrontal cortex supports core executive processes such as cognitive control, value integration, and strategic regulation, which are essential for navigating cooperative and competitive interactions. Accordingly, the present study focused on frontal regions to investigate the neural mechanisms underlying cognitive control and value negotiation during joint decision-making. Concentrating on this task-relevant network reduced multi-region sampling noise and enabled a more targeted and rigorous characterization of inter-brain coupling in the prefrontal cortex. Some recent work suggests that competition heightens activation in reward-related circuits, whereas cooperation is associated with greater orbitofrontal and ventromedial prefrontal activity (Knyazev et al., 2024), indicating that neural encoding of outcomes depends on social context. However, most of these studies analyze single brains in isolation, neglecting the inherently interactive nature of social decisions. fNIRS hyperscanning directly addresses this limitation by enabling the simultaneous recording of cortical hemodynamics from multiple individuals during naturalistic interactions. Accumulating evidence indicates that cooperation and competition modulate inter-brain synchrony (IBS) in the dorsolateral prefrontal cortex (DLPFC) and frontopolar cortex (FPC), with effects influenced by task structure, interpersonal context, and participant characteristics (Peng et al., 2025; Song et al., 2024; Yin, 2025). Importantly, recent hyperscanning research has distinguished cooperative and competitive decision-making into two primary interaction modes, simultaneous and turn-based, each engaging distinct cognitive and neural processes. For example, using a turn-based Balloon Analogue Risk Task (BART), Zhao et al. (2023) demonstrated that IBS in frontopolar and inferior frontal regions dynamically tracked risk-taking behavior between friends and strangers, reflecting real-time adaptation to social feedback. These findings suggest that turn-based decision-making offers a unique window into the temporal dynamics of mutual influence, whereby each individual's behavior continuously shapes the partner's subsequent choices.

Within this growing literature, converging evidence further suggests that IBS is frequency-dependent. For instance, in the Iowa Gambling Task (IGT), competition has been shown to increase IBS in male dyads, whereas cooperation enhances IBS in female dyads within a low-frequency range (Peng et al., 2025). Such results align with broader findings that low-frequency hemodynamic synchrony (~0.01–0.1 Hz) captures slow, socially driven neural dynamics associated with sustained coordination and shared task engagement (Nguyen et al., 2021; Park et al., 2023). In parallel, hyperscanning studies have repeatedly reported gender-related differences in both behavioral alignment and brain-to-brain synchrony during collaborative tasks, with female dyads often exhibiting stronger interpersonal coordination (Baker et al., 2016; Lu et al., 2020a). Given the established differences in neural and behavioral strategies, restricting the sample to female participants allowed us to focus on a more homogeneous interaction pattern and reduce potential confounding effects of gender variability, thereby enhancing the internal validity of the present investigation into social decision-making.

More broadly, emerging evidence suggests that different frequency bands of inter brain synchrony may reflect distinct cognitive and neural processes, with ultra slow fluctuations reflecting sustained social monitoring or responsibility diffusion, and higher frequencies reflecting rapid reward based updating and decision adjustment. (e.g., Guglielmini et al., 2022). Ignoring this spectral diversity risks conflating separable mechanisms into a single averaged IBS measure. A recent framework has extended Wavelet Transform Coherence to examine cross-frequency, time-dependent coupling across brain–brain, brain–body, and body–-body systems (Guglielmini et al., 2022), underscoring the need to interpret IBS metrics across frequency bands. Nevertheless, empirical work directly linking frequency-specific IBS measured with fNIRS to reinforcement learning processes remains limited. Building on accumulating evidence for the functional relevance of distinct hemodynamic frequency bands (Peng et al., 2025; Zhang et al., 2024; Zhao et al., 2023), the present study examines how frequency-resolved IBS relates to latent reinforcement learning variables, providing an initial step toward integrating spectral neural coupling with computational models of social decision-making.

In this study, we adopted a data-driven approach to identify frequencies of interest (FOIs) and, importantly, detected an additional FOI beyond those typically reported. This finding expands the spectral characterization of prefrontal coupling and allows us to examine whether specific FOIs correspond to distinct reinforcement learning (RL) parameters. By linking frequency-specific IBS patterns to RL-derived cognitive markers such as reward-frequency sensitivity and choice flexibility, we aim to provide a mechanistic account of how social contexts shape adaptive decision strategies. To address these questions, we combined fNIRS hyperscanning with RL modeling in both turn-based cooperative and competitive variants of the IGT. Focusing on the prefrontal cortex as our region of interest, we investigated: (i) whether RL parameters can serve as computational markers of social-context adaptation; and (ii) how frequency-specific IBS relates to these parameters and to decision outcomes. We further compared five RL models (EV, PVL_delta, ORL, VPP, VSE) to determine the optimal fit for dyadic decision-making. Based on the above analysis, we propose the following hypotheses:

H1. RL parameters capture systematic differences in learning strategies between cooperation and competition.

H2. Frequency-specific IBS in prefrontal regions, in combination with RL parameters, explains variability in decision-making performance.

H3. Competition enhances performance via DLPFC-mediated reward sensitivity (H3a), whereas cooperation reduces performance via FPC-mediated cognitive load associated with coordination (H3b).

Table 1
The potential gains and losses per deck in one block.

Deck	Deck's earning in one block (*10 trials*)										Final earnings	Types
	Trial1	Trial2	Trial3	Trial4	Trial5	Trial6	Trial7	Trial8	Trial9	Trial10		
1	100	100	100	−1250	100	100	100	100	100	100	−250	Bad
2	100	−200	100	−250	−250	100	−300	100	−250	100	−250	Bad
3	50	50	−250	50	50	50	50	50	50	50	250	Good
4	50	−75	50	50	−75	−100	50	50	50	50	250	Good

Note: This table presents an example block. Throughout the entire experiment, the gain/loss settings for trials varied across different blocks. However, the block-level gain of each deck remained fixed: Deck 1 and Deck 2 yielded a loss of 250, and both Deck 3 and Deck 4 yielded a gain of 250.

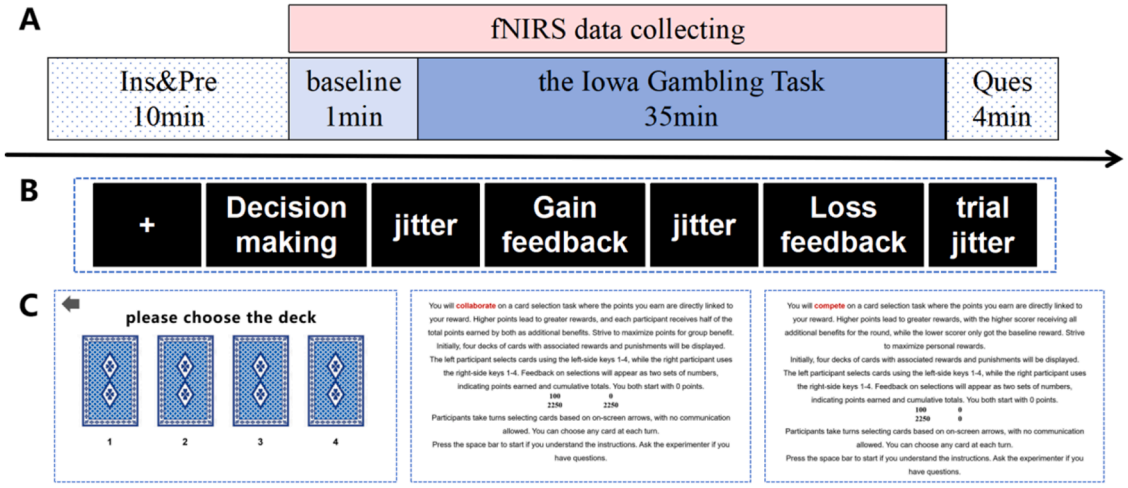

Fig. 1. Experimental Paradigm and Task Design. (A) Schematic representation of the overall experimental procedure. (B) Trial structure and temporal sequence of the dyadic risky decision-making task. (C) Instructional guidelines for the cooperative and competitive interaction contexts.

2. Methods

2.1. Participants

This study employed G*Power 3.1.9.7 to conduct an a priori power analysis (Faul et al., 2007), which indicated that a sample of 58 dyads was required to detect an effect size of 0.35 (Cohen's f = 0.35; α = 0.05; power = 0.85). A total of 128 female participants were recruited and randomly assigned into 64 previously unacquainted dyads. These dyads were then randomly allocated to either a competitive condition (n = 32) or a cooperative condition (n = 32). Four dyads were excluded due to data corruption and missing trials, resulting in 60 dyads being included in the final analyses (n_{coop} = 30, n_{comp} = 30). The two groups were closely matched in age ($M_{coop} \pm SD$ = 20.40 ± 1.78; $M_{comp} \pm SD$ = 20.50 ± 1.94), with no significant inter-group difference (Mann-Whitney U = 446.50, p = 0.983). Given this high degree of demographic homogeneity, age was not included as a covariate in the primary General Linear Models (GLM) to prioritize model parsimony and preserve degrees of freedom. Nonetheless, to evaluate the robustness of our findings, we conducted supplementary Analyses of Covariance (ANCOVA) with age as a covariate. These sensitivity analyses yielded results consistent with our primary findings, confirming that the observed IBS and behavioral effects were not driven by age-related variance (detailed in Supplementary Material S3). Handedness was not treated as a covariate as all participants were verified as right-handed through verbal screening based on the Edinburgh Handedness Inventory criteria, rendering the variable a constant across the sample. Rigorous pre-screening ensured that all participants were in sound mental and physical health, with no history of neurological or psychiatric disorders. Prior to the formal experiment, current health status (e.g., fatigue levels and sleep duration) was verified. All participants provided written informed consent and were compensated with performance-based monetary rewards. The study adhered to the principles outlined in the Declaration of Helsinki and received approval from the Institutional Review Board of the Academic Committee of Key Laboratory of Brain-Machine Intelligence for Information Behavior at Shanghai International Studies University in China.

2.2. Task and procedure

2.2.1. The Iowa Gambling Task within social interaction

Building on previous research, this study adapted the IGT for two-person scenarios, incorporating monetary rewards and feedback mechanisms to distinguish between cooperation and competition. The task comprised 10 blocks of 20 trials each, totaling 200 trials, with participants completing 100 trials independently. In each trial, participants alternated between roles as decision-maker and observer, with the decision-maker choosing one card from four decks, each characterized by unique reward and penalty structures (Zhao et al., 2022, 2023). In this study, the decision maker uses decal-marked keyboard keys to make the selection to regulate the influence of key positions and the original keyboard functionality on decision-making. The initial decision-maker was determined through a randomized procedure, indicated by a grey arrow, with subsequent assignments alternating between participants. The payoff structure of the four decks within each participant's trials mirrored the standard IGT (Schmitz et al., 2018; Zhang et al., 2023a), featuring two "bad" decks and two "good" decks. Importantly, the payoffs were independent for each participant within a dyad, ensuring that one participant's decisions did not affect the other's earnings, which facilitated a direct comparison of decision-making performance in both cooperative and competitive contexts.

Each trial included a fixation screen (0.5 s), a decision screen (≤15 s), and feedback screens for gains and losses (2 s). Participants were informed that each deck entailed potential gains and losses, while the

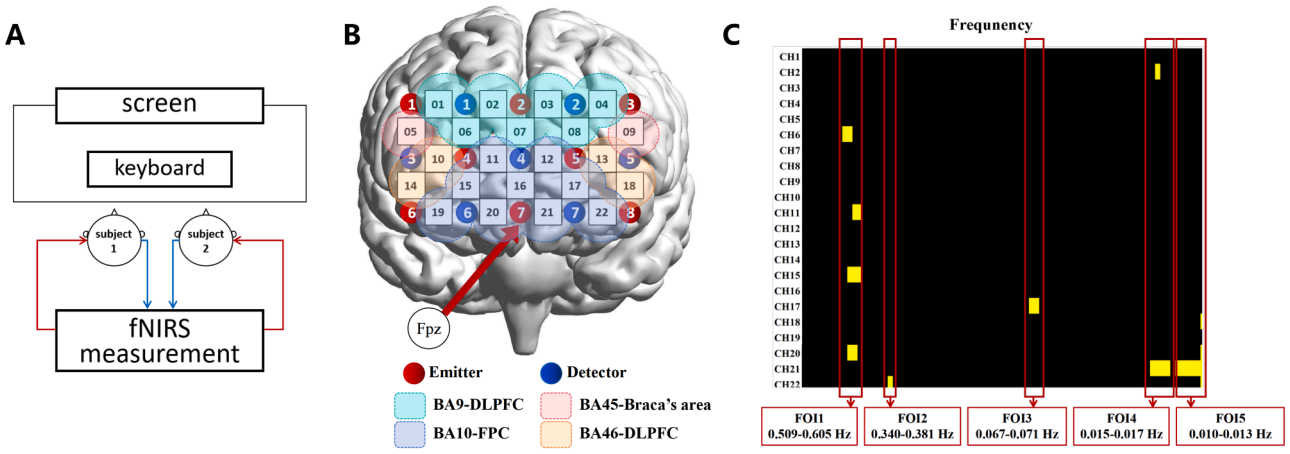

Fig. 2. Neuroimaging data acquisition and spectral parcellation. (A) Schematic of the hyperscanning setup, illustrating the experimental data collection scenario for dyadic interaction. (B) Optode configuration and topographic mapping, with probe locations defined according to the MNI coordinate system. The probe layout was visualized using BrainNet Viewer based on the optode localization and brain region distribution information output by NIRS_SPM. To more clearly illustrate the localization relationship between channels and corresponding brain regions, dotted shapes of different colors were plotted to represent the distribution of brain regions associated with each channel. (C) Frequency-of-Interest (FOI) identification via FDR-corrected p-value maps. The panels from left to right display the statistical significance maps for FOI1 through FOI5, respectively.

specific Settings (see Table 1) were not directly disclosed and they needed to conduct their own observations and summaries (consistent with previous studies). To mitigate fatigue and match hemodynamic response dynamics, a randomized time interval (0.8–1.2 s) was jittered between key screens within a trial, and inter-trial intervals (ITI) varied from 2–4 s post-loss feedback. Other experimental parameters adhered to established protocols from former fNIRS-based IGT studies (León, 2023; Li, 2019). The cooperative or competitive context was manipulated by the instruction, the monetary incentives (Horn and Freund, 2021; Liu et al., 2020; Wu et al., 2023; Xu et al., 2016) and the feedback screen presentations (see more details in Fig. 1). Specifically, participants were simultaneously informed that the task required either cooperation or competition and that their earnings would directly determine their final remuneration via on-screen written instructions and oral explanations from an experimenter. In both conditions, each participant received a base payment of 30 CNY, with the primary source of payoff differentiation residing in the allocation rule governing the bonus payment. In the cooperative condition, participants shared earnings and the bonus, and the feedback screen displayed the cumulative earnings of dyad. The higher the cumulative earnings, the larger the bonus (range: 0–70 CNY), which was split equally between the two members. In the competitive condition, earnings were independent, and the feedback screen presented each participant's separate cumulative earnings. At the end of the task, the individual with the higher cumulative earnings received the entire bonus (35 CNY), whereas the individual with the lower cumulative earnings retained only the 30 CNY base payment.

2.2.2. Experimental procedure

Upon arrival, participants were required to complete an informed consent form and verbal checks covering general health, recent psychological/mental status, and handedness. Two participants sat side-by-side in front of a shared computer monitor. After a brief overview and practice session to ensure task understanding, participants were fitted with fNIRS caps. The data-collection protocol began with resting-state measurements, during which participants were instructed to maintain closed eyes and remain stationary for one minute, specifically avoiding both physical movement and mental exertion. Neuroactivity was then recorded during the modified IGT task. The resting-state data were subtracted from task-phase data to establish baseline-corrected task-state data for subsequent analysis. Verbal communication was not allowed during the experiment.

2.3. fNIRS data acquisition

Given the prefrontal cortex's crucial role in decision-making, social cognition, and other executive functions (Yang et al., 2020), it was designated as the region of interest (ROI) for this study. An fNIRS optical topography system (LABNIRS, Shimadzu Corporation, Japan) utilizing a three-wavelength near-infrared semiconductor laser (780 nm, 805 nm, 830 nm) was employed to synchronously record oxygenated and deoxygenated hemoglobin levels in the PFC of participants in each dyad, based on the modified Beer-Lambert law (Scholkmann et al., 2014; Wang et al., 2017; Zhao et al., 2022). The sampling rate was set at 10 Hz (Xue et al., 2018). For each participant, a 3 × 5 photoelectric probe set which contained 8 emitters and 7 detectors spaced 30 mm apart was placed over the PFC region with Fpz as the reference, referring to the international 10–20 system (Zhao et al., 2023). This probe set comprised 22 channels (CHs). The middle row of the photoelectric probe set was aligned with the sagittal plane, while the bottom row was aligned with the axial plane (see Fig. 2). The more detail of MNI coordinates of the optode layout was showed in Supplementary Material S2.

The spatial anatomical positions of the 22 channels were determined using the virtual spatial registration function of the Polhemus Fastrak 3D Digitizer (Lu et al., 2023; Song et al., 2024). The corresponding Montreal Neurological Institute (MNI) coordinates were calculated using NIRS_SPM MATLAB packages, referencing Nz, Cz, AL, and AR positions (Tsuzuki et al., 2007; Ye et al., 2009).

2.4. Data analysis

2.4.1. Behavior data analysis

Conforming to prior research, cumulative earnings and net score were used to assess dyadic decision-making performance (Zanini et al., 2024). Specifically, cumulative earnings are the total value a participant gains (after deducting losses) via all card selections, and the net score is calculated by subtracting selections from disadvantageous decks (Decks 1, 2) from those from advantageous decks (Decks 3, 4) to measure decision-making performance. A repeated ANOVA (group × block) was conducted on the cumulative earnings and the net score to test for group differences across the 5 blocks.

2.4.2. Computational cognitive model of the IGT task in dyads

The computational cognitive model fitting and comparison. In the present study, model fitting and comparison across the five models

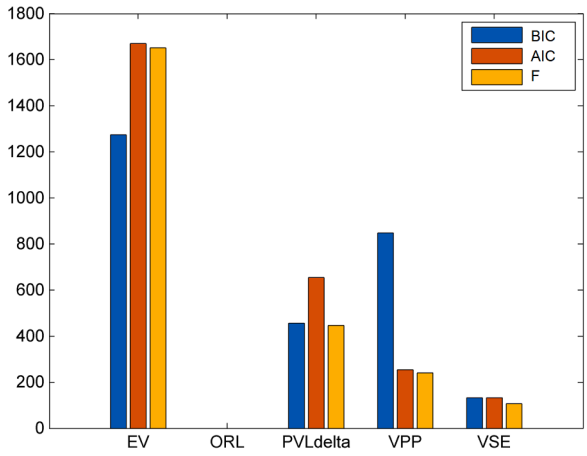

Fig. 3. Formal model comparison across five reinforcement learning architectures. Model fit was evaluated using the Bayesian Information Criterion (BIC), Akaike Information Criterion (AIC), and the Free Energy (F) metric. For intuitive visualization, the ORL model is defined as the baseline (benchmark), and the y-axis represents the relative difference in fit metrics (△BIC, △AIC, and △F) for each alternative model compared to the ORL model. Lower values indicate superior model fit. The ORL model consistently exhibited the most robust performance across all evaluation criteria.

mentioned above (EV, PVL_delta, ORL, VPP, and VSE) was performed utilizing a MATLAB toolbox (https://github.com/romainligneul/igt-toolbox) proposed by Ligneul and the VBA MATLAB toolbox (Daunizeau and Ligneul, 2019; Morel, 2018; Prlic et al., 2014). The model configurations in this study are consistent with those in the existing literature, which has provided an exhaustive description of the aforementioned model configurations (Daunizeau and Ligneul, 2019; Haines et al., 2018; Steingroever et al., 2016; Wetzels et al., 2010). To evaluate model fit, we employed the Bayesian Information Criterion (BIC), Akaike Information Criterion (AIC), and Free Energy (F) as metrics to assess the fit of the five models. Lower values of these criteria indicate better model fit (Alibakhshi and Hartke, 2021; Fukushima and Yoshidome, 2023; Lv and Liu, 2014). Similar to the AIC and BIC methodologies, minimizing free energy leads to optimal model configurations (Bogacz, 2017; Buckley et al., 2017). The empirical analysis revealed that the ORL model exhibits the most optimal fitting performance, followed by the VSE model ($DIFF_{AIC}$=133.487, $DIFF_{BIC}$=133.487, $DIFF_{F}$=107.446). According to previous research, a discrepancy of greater than 100 between the indicators of two models indicates that the selection of an inadequately fitting model would result in an unacceptable loss of information (Daunizeau and Ligneul, 2019). It can thus be concluded that the ORL model represents the optimal fit model in the context of the two-person joint IGT task. The comparative results of model fits are shown in Fig. 3.

The computational cognitive model comparison and recovery. The Bayesian group comparisons for the three fitted metrics, AIC, BIC, and F, were performed with the assistance of VBA and the igt_toolbox Matlab toolbox (Daunizeau and Ligneul, 2019; Prlic et al., 2014; Stephan et al., 2009). These analytical procedures were grounded in the logit evidence for each model, and the models were attributed as random effects. Subsequently, simulated analysis including predictive performance, parameter recovery, and model recovery were conducted on the five models based on a series of simulated data (Chen, 2021; Palminteri et al., 2017; Spektor and Kellen, 2018; Steingroever et al., 2018).

The empirical findings from the Bayesian group comparison showed that the estimated model frequencies of the ORL, and VSE models were both above chance level. The ORL model demonstrated higher estimated model frequencies than the other models on all three measures (approximated exceedance probabilities between 0.6 and 0.8), with the VSE model exhibiting the second-highest frequency (see Fig. 4).

In addition, the results of the fitted choices demonstrate that the ORL, VPP and VSE models manifested the highest degree of predictive accuracy, with the EV and PVL models exhibiting a comparatively lower level of performance. Furthermore, the results of the simulated choices showed that the VSE model achieved the highest prediction accuracy, followed by the ORL model. This suggests that the ORL and VSE models are more effective in accurately predicting dyadic pairwise decisions (for further details, please refer to Fig. 5 and Table 2).

Moreover, as showed in the linear regression of parameter recovery, the ORL model exhibited the most robust parameter stability among 5 models, followed by the VPP and VSE models (See Fig. 6).

Similarly, model recovery results showed that the VSE model demonstrated the best general stability, in that the simulation data obtained through the optimal fitting parameters of the VSE model continued to perform best when the model was re-fitted. The PVL, ORL, and EV models exhibited the next best performance, and to some extent still demonstrated model stability in describing dyadic pairs in the decision-making task. However, they showed poor fit consistency on some metrics (e.g., the EV model performing slightly worse on the F metric). The VPP model performed the worst on the BIC metric, suggesting that its fitting ability needs to be considered carefully (see Fig. 7).

Taken together, the results of the model fitting and comparison process indicate that the ORL model demonstrates the optimal performance, suggesting that dyads may integrates cognitive processes such as expected value learning, win frequency learning, reversal learning, and choice persistence to predict and explain choices in the IGT. Specifically, the ORL model comprises five parameters: the positive outcome learning rate (α_{Rew}) and negative outcome learning rate (α_{Pun}) represent the decision-maker's sensitivity to positive and negative outcomes, respectively; the choice persistence decay parameter (K) indicates the decision-maker's memory retention of past choices; the win-frequency weight (β_{fre}) and choice persistence weight (β_{per}) represent the influence of win frequency and choice persistence on the total value. See Table 3 for the specific parameter settings and their meanings within the model. In an analysis section below, we report an evaluation of the existence of between-group differences in these aforementioned model parameters using independent samples *t*-tests with GROUP as the independent variable, as postulated by the ORL model of optimal performance.

2.4.3. fNIRS data analysis

Preprocessing on the individual level fNIRS data. Expanding on prior research, this study used a two-step method to assess fNIRS data quality (Lu et al., 2020b; Sun et al., 2021). Initially, channel data were visually inspected for anomalies during hyperscanning, with flagged channels plotted using MATLAB's NIRS-SPM toolbox. Channels lacking the characteristic 1 Hz heartbeat signal (Nguyen et al., 2021) were deemed "bad" and replaced with the mean of adjacent channels (Zhao et al., 2022). Three dyads were excluded for poor signal quality or corruption; others were excluded for missing a trial in the decision-making task, leaving 60 dyads for final analysis.

The raw data of rest dyads were preprocessed using the NIRS_SPM package, applying HRF low-pass filtering to address temporal autocorrelation and Wavelet-MDL detrending to remove motion and other artifacts (Bulgarelli, 2018; Ye et al., 2009). Following previous fNIRS hyperscanning studies, only the hemoglobin oxygenation (HbO) signal, which is sensitive to cortical blood flow changes, was analyzed (Hou et al., 2022; Jiang et al., 2015).

Preprocessing IBS at the dyad level. Based on previous research, we utilized a MATLAB package to compute inter-brain synchrony in decision-making and feedback phases through a Wavelet Transform Coherence approach (Grinsted et al., 2004). The calculation formula for the Wavelet Transform Coherence of the HBO signals is presented below, in which "n" represents time, "s" represents a wavelet scale, "i" and "j" represent the signals of dyads, "W^i" or "W^j" represent the continuous wavelet transform of two participants, and "W^{ij}" represents the

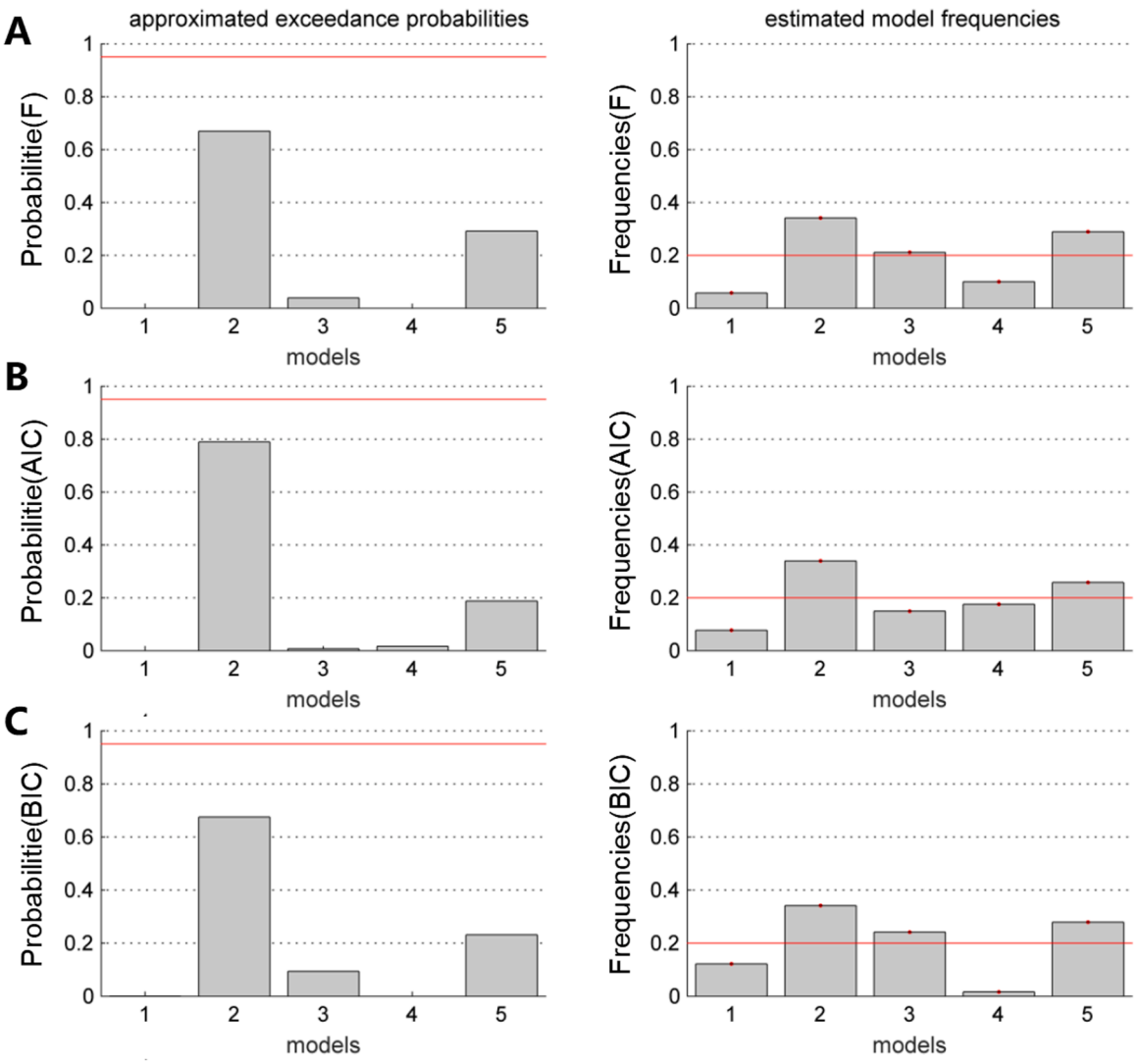

Fig. 4. The Bayesian Group Comparison, where models 1–5 represent EV, ORL, PVL-delta, VPP, and VSE, respectively. This figure shows the approximated exceedance probabilities and the estimated model frequencies based on F (A), AIC (B), and BIC (C). The red line represents the ideal approximated exceedance probabilities (*ep*) and the estimated model frequencies (*emf*). *ep* is the probability that a certain model is more likely to be the "optimal model" compared to all other candidate models which threshold is 0.99. *emf* is the proportion of times this model is determined as the optimal model among all participants (the estimated frequency of the ORL model is all > 30%). As shown above, the ORL model exhibited the best performance among the five models.

cross-wavelet transform of two participants (Hou et al., 2020; Nozawa et al., 2016; Zhao, 2021).

$$WTC(n,s) = \frac{\left|\left\langle s^{-1}W^{ij}(n,s)\right\rangle\right|^2}{\left|\left\langle s^{-1}W^{i}(n,s)\right\rangle\right|^2\left|\left\langle s^{-1}W^{j}(n,s)\right\rangle\right|^2}$$

The FOI of IBS was identified first (Jin et al., 2024; Liang et al., 2022). Focusing on decision making under social interaction, data were restricted to 0.01–1 Hz (Liu, 2023; Zhang et al., 2023a), excluding physiological noise bands (0.03–0.06 Hz and 0.08–0.12 Hz for blood pressure, 0.15–0.3 Hz for respiration, and 0.7–1.0 Hz for cardiac activity) (Li et al., 2024; Rieger et al., 2018; Zheng et al., 2018). Prompted by recent work extending neural-coupling analyses from 0.01 to 0.2 Hz up to 1 Hz—and in some cases 5 Hz—we slightly expanded the traditional frequency-of-interest (FOI) window to achieve a more comprehensive characterization of the neural underpinnings of social risk decision-making (Cheng et al., 2022; Zhao et al., 2023). To minimize physiological contamination from respiration (~0.2–0.3 Hz) and cardiac activity (~0.7–1 Hz), previous studies routinely excluded these bands (Yin, 2025; Zhang et al., 2021, Zhang et al., 2019) and confined the FOI to 0.01–0.2 Hz, consequently restricting most reported effects to this low-frequency range. We reasoned that modestly higher, yet still non-physiological, bands (e.g., 0.3–0.6 Hz) might carry additional interpretable information. Moreover, our protocol introduced a minor adaptation to the standard joint-decision paradigm: participants were required to divide labor and make independent choices under both cooperative and competitive incentives. Thus, after rigorously removing established physiological bands, we shifted the analytical focus to these under-explored higher frequencies, hoping to provide complementary evidence that differentiates cooperative from competitive risk decisions.

After baseline correction with 1 min resting-state data (Tang et al., 2016), task-related coherence values were transformed into Fisher z-statistics (Zhang et al., 2024; Zhou, 2022). A series of one-sample *t*-tests that were FDR-corrected (using the Benjamini–Hochberg procedure) were performed on the Fisher's Z statistics across all 80 frequency bins to identify the FOI. Five distinct FOI bands were identified (FDR-corrected $p < 0.05$, see Fig. 2C), including: (1) 0.010–0.013 Hz; (2) 0.015–0.017 Hz; (3) 0.067–0.071 Hz; (4) 0.340–0.381 Hz; and (5) 0.509–0.605 Hz. Ultimately, a series of FDR-corrected (Benjamini–Hochberg procedure) repeated-measures ANOVAs assessed group differences on FOIs, with group (cooperation, competition) as the

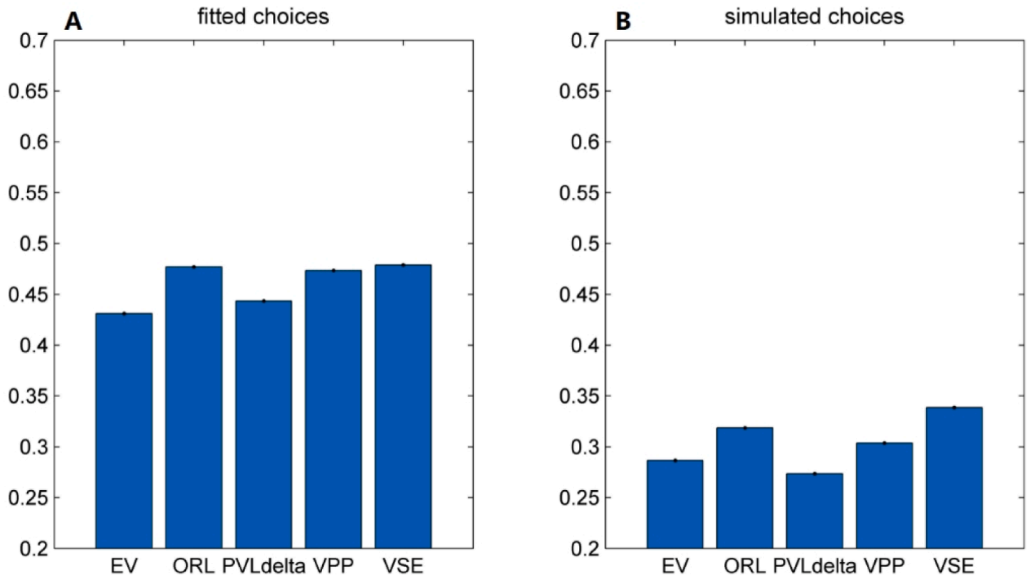

Fig. 5. The predictive accuracy of models for fitted data (A) and simulated data (B). Note that the higher the values of these bars are, the better the predictive accuracy is. As shown above, the VSE and ORL model exhibited the most robust predictive accuracy among other models.

Table 2
Predictive accuracy of all models in fitted and simulated data.

Model	Fitted ($M \pm SD$)	Simulation ($M \pm SD$)
EV	0.431±0.015	0.287±0.008
ORL	0.477±0.014	0.319±0.010
PVL_delta	0.443±0.015	0.274±0.008
VPP	0.473±0.013	0.304±0.009
VSE	0.479±0.014	0.339±0.009

between-variable and STAGE (decision-making, feedback) as the within-variable (Sun et al., 2021). BrainNet Viewer MATLAB package was utilized for visualization (Xia et al., 2013).

To further examine the robustness of our findings, we conducted 1000 permutation tests on the significant WTC results. Given that the data sampling points varied across participant pairs (determined by participants' decision times), we adopted a data-specific permutation approach for significant interaction effects (Feng et al., 2025). Specifically, we randomly shuffled the 200-trial data from one participant for each pair and recomputed the WTC values with the other participant. After baseline correction and Fisher's Z transformation, permutation tests were performed. This procedure disrupted the true interactive states while preserving the internal coherence of trial-level data. For significant between-group main effects, we permuted group labels 1000

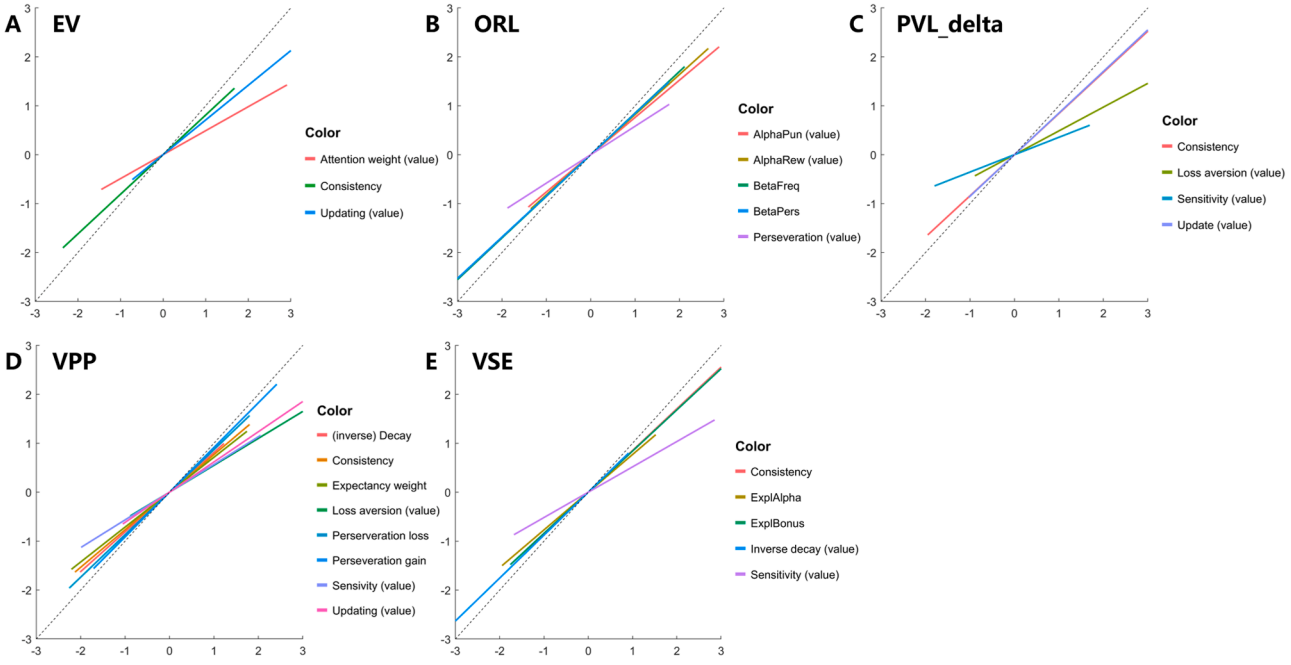

Fig. 6. The parameter recovery results of the five models, including the parameter regression lines of (A) the EV model, (B) the ORL model, (C) the PVL_delta model, (D) the VPP model, (E) the VSE model. Here the grey dashed line represents the regression line where the fitted and simulated parameters are equal, and the closer the parameters line are to the grey dashed line, the better the parameter recovery results are. As shown above, the ORL model exhibited the most robust parameter stability among the five models, followed by the VPP and VSE models.

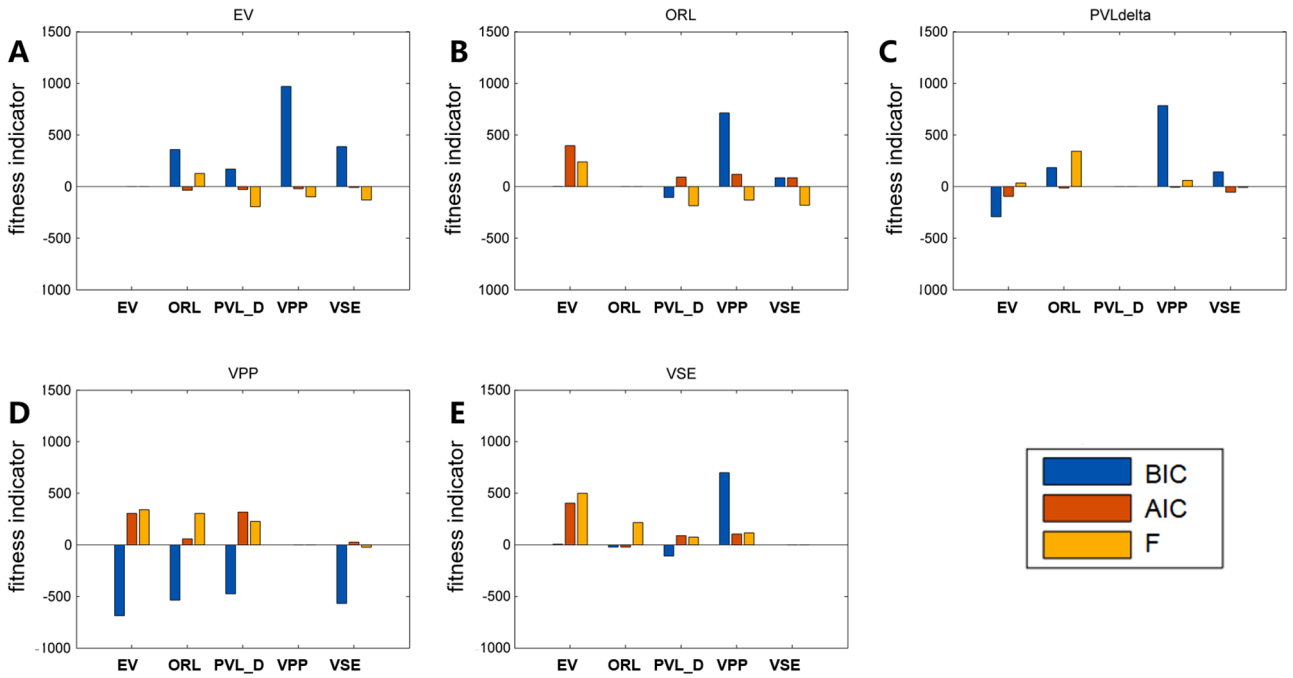

Fig. 7. The model recovery results, including the recovery bar plots with (A) the EV model, (B) the ORL model, (C) the PVL_delta model, (D) the VPP model, (E) the VSE model as the baseline model. All bars with values less than zero indicate that, compared to the original model used to generate these simulation data, other models can better explain the simulation data, suggesting poor model recovery capacity of the original model. As shown in the plot, the VSE and ORL model exhibited the most robust model stability among other models, followed by the PVL_delta and EV model.

Table 3
The parameter settings and equations of ORL.

Parameter	Equation	Function
α_{REW}	$EV_j(t+1) = EV_j(t) + A_{rew}\cdot(x(t) - EV_j(t))$	capture differential sensitivities to losses and gains
α_{PUN}	$EV_j(t+1) = EV_j(t) + A_{pun}\cdot(x(t) - EV_j(t))$	capture differential sensitivities to losses and gains
β_P	$V_j(t+1) = EV_j(t+1) + EF_j(t+1)\cdot\beta_F + PS_j(t+1)\cdot\beta_P$ Both free parameters in the function	$\beta_P > 0$, tend to stick to previous choices (persist); $\beta_P < 0$, tend to switch and select (explore); $\beta_P = 0$, previous choices do not affect current decisions;
β_F		$\beta_F > 0$, preference high win rate deck; $\beta_F < 0$, preference low win rate deck.
K	$PS_j(t+1) = \frac{1}{1+K}$ (choosen) ; $PS_j(t+1) = \frac{PS_j(t)}{1+K}$ (unchoosen)	a reversal learning component to update the expected outcome frequency of unchosen decks

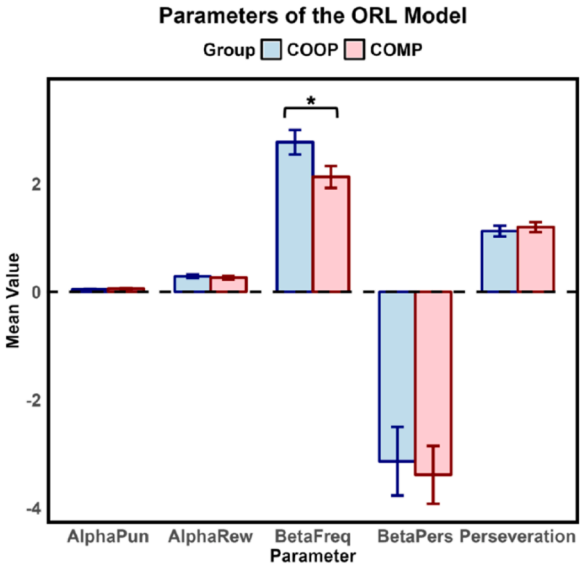

Fig. 8. The between-group differences in the parameters of the ORL model. BetaFreq (β_{fre}) refers to the decision weight of the deck win frequency. Bars represent *mean* ± *SEM*. * means FDR-corrected $p < 0.05$.

times to precisely assess the authentic group effects. Furthermore, we conducted 1000 permutation tests based on frequency-band-by-channel clustering, wherein continuous frequency bands and spatially clustered channels were treated as a single cluster. Detailed procedures and results are provided in Supplementary Material S1.

The coupling directionality on the dyad level. To deepen understanding of dyadic decision-making neural substrates, we utilized Granger causality analysis (GCA) to investigate directed interbrain connections (Bressler and Seth, 2011; Granger, 1969; Im et al., 2010), which has been effective in uncovering neural signal directionality in social contexts (Chen, 2022; Pan et al., 2017; Zhang et al., 2023b). The GCA procedure in this study included: extracting fNIRS data from IGT task phases with significant group differences using MATLAB, calculating trial means to standardize data, and employing the HERMES package to determine pairwise causalities (Chen, 2020; Zhang et al., 2023c).

The GC index calculation for the y to x direction is detailed subsequently.

$$GC_{y\to x} = \ln\left(\frac{V_{x|\bar{x}}}{V_{x|\bar{x}\bar{y}}}\right)$$

Table 4
ANOVA Results for IBS.

Channel	MAIN effect				INTERACTION effect	
	STAGE		GROUP		STAGE × GROUP	
	F value	*p* value	*F* value	*p* value	*F* value	*p* value
CH4-FOI4	1.480	0.229	0.549	0.462	**11.80**	**0.001**
CH6-FOI2	0.140	0.710	0.917	0.342	**12.358**	**<0.001**
CH12-FOI2	2.530	0.117	**9.280**	**0.003**	1.880	0.176
CH20-FOI2	1.360	0.249	**9.920**	**0.003**	3.040	0.087
CH21-FOI2	0.702	0.405	**9.390**	**0.003**	2.366	0.129

Note: This table presents the ANOVA results for all IBS target channels. The frequency band for FOI2 ranges from 0.340 to 0.381 Hz, while the frequency band for FOI4 ranges from 0.015 to 0.017 Hz. The significant effects are bold-faced on light gray.

According to this calculation, the numerator is the variance of the residuals when x is predicted using only the past values of x, and the denominator is the variance of the residuals when x is predicted using both the past values of x and y. The denominator is the variance of the residuals when x is predicted using both the past values of x and y.

$$V_{x|\bar{x}\bar{y}} = \mathrm{var}(u_{xy})$$

The time series x is similarly calculated as shown below. The fNIRS time series of one participant y (n) into the bivariate autoregressive model of the fNIRS time series of the other participant x (n) is also denoted below (Nisoet al., 2013).

$$x(n) = \sum_{k=1}^{p} a_{x|x,k} x_{(n-k)} + \sum_{k=1}^{p} a_{x|y,k} y_{(n-k)} + u_{xy}(n)$$

A three-factor repeated measures ANOVA tested for GROUP, STAGE, and DIRECTION effects.

2.4.4. Pearson correlations: reconciling cognitive models with neurobiological evidence

Pearson correlations were used to explore relationships between behavior, cognition, and neural activity in dyadic decision-making, focusing on significant IBS channels, model parameters, and IGT metrics.

3. Results

3.1. Behavioral performance in the IGT

The repeated measured ANOVA with GROUP (coop and comp) as a between-participant factor and BLOCK (B1, B2, B3, B4, and B5) as a within-participant factor was conducted on the accumulative earnings and net scores to test the group difference on the IGT task among the 5 blocks. Results of accumulative earnings showed a significant main effect of BLOCK, F (4, 232) = 5.27, $p < 0.001$, $\eta_p^2 = 0.083$. Subsequent simple effects analyses found that accumulative earnings at B1 ($p < 0.01$) and B2 ($p < 0.05$) were significantly lower than that at B5. There was also a significant main effect of GROUP, F (1, 58) = 94.60, $p < 0.001$, $\eta_p^2 = 0.620$. Following simple effects analyses, it found that the accumulative earnings of the COMP group was significantly higher than that of the COOP group. The interaction effect on accumulative earnings was not significant, F (4, 232) = 1.01, $p = 0.401$, $\eta_p^2 = 0.017$.

The analysis of net scores showed a significant main effect of BLOCK, F (4, 232) = 6.964, $p < 0.001$, $\eta_p^2 = 0.107$. Following simple effects

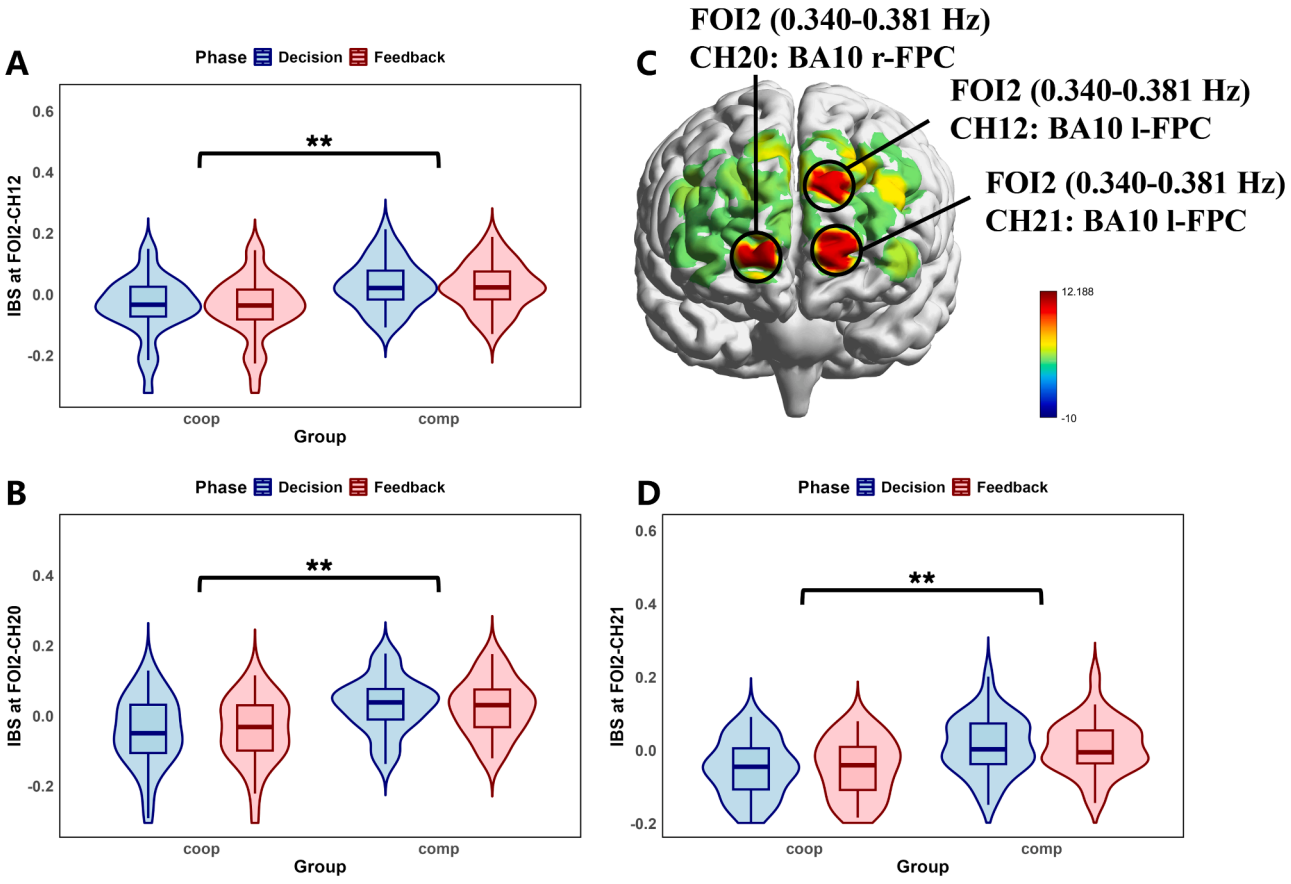

Fig. 9. Group differences in IBS at FOI2 in FPC channels. (A) CH12 (BA10), (B) CH20 (BA10), and (D) CH21 (BA10) all showed significantly higher IBS in the COMP group than in the COOP group (all FDR-corrected $p < 0.01$). (C) Schematic illustration of the ANOVA results. A schematic illustration including Brodmann Area annotations is shown in Figure S5C. Data are averaged across decision-making and feedback stages. Bars represent *Mean* ± *SEM*. ** means FDR-corrected $p < 0.01$.

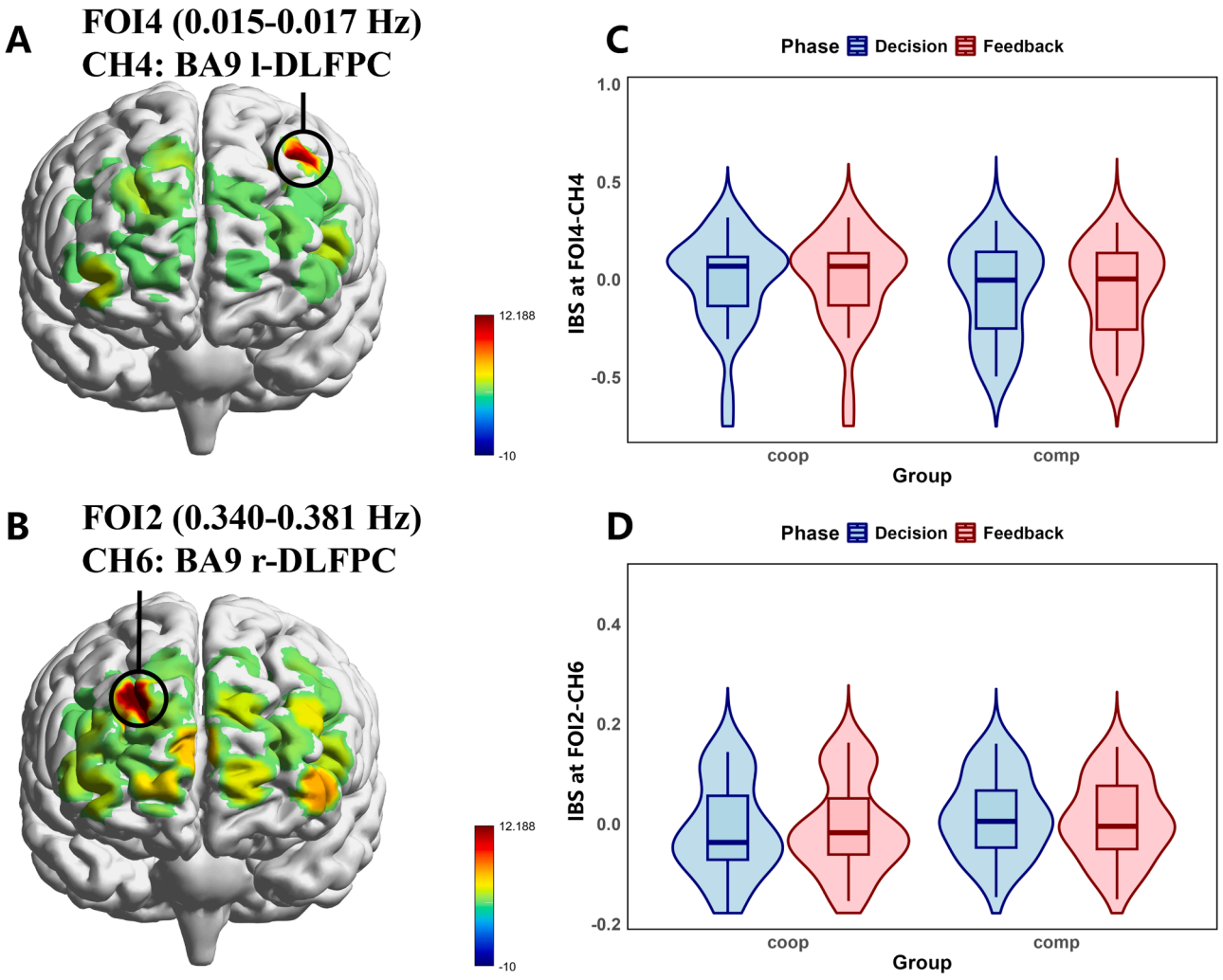

Fig. 10. Stage-dependent effects on IBS in DLPFC channels at FOI2 and FOI4. (A) Schematic illustration of the interaction effect in FOI4. A schematic illustration including Brodmann Area annotations is shown in Figure S6A. As shown in panel (C), a significant GROUP × STAGE interaction was observed for CH4 (BA9) at FOI4 (FDR-corrected $p < 0.05$), with the COMP group showing higher IBS during decision-making than feedback (FDR-corrected $p < 0.05$). (B) Schematic illustration of the interaction effect in FOI2. A schematic illustration including Brodmann Area annotations is shown in Figure S6B. As shown in panel (D), CH6 (BA9) at FOI2 also showed a significant GROUP × STAGE interaction (FDR-corrected $p < 0.001$), with the COMP group showing greater IBS during decision-making than feedback (FDR-corrected $p < 0.05$). Bars represent *Mean* ± *SEM*. * means FDR-corrected $p < 0.05$; ** means FDR-corrected $p < 0.01$.

analyses it was found that the net scores at B5 were significantly higher than those at B2 ($p < 0.01$) and B3 ($p < 0.05$). In addition, the net scores at B4 were significantly higher than those at B2 ($p < 0.01$). The main effect of GROUP ($F_{(4,\ 232)} = 1.44$, $p = 0.235$, $\eta_p^2 = 0.024$) and the interaction effect ($F_{(4,\ 232)} = 0.914$, $p = 0.456$, $\eta_p^2 = 0.016$) were both not significant.

3.2. Computational cognitive modelling in the IGT

As for the computational cognitive modelling results showed in Fig. 8, an independent samples *t*-test was conducted with GROUP as the independent variable and with win-frequency sensitivity (β_{fre}) as the dependent variable. This revealed that the β_{fre} of the COMP group was significantly lower than that of the COOP group ($t = 2.101$, $p < 0.05$, Cohen's d = 0.543). This finding suggests that the COOP group prioritized deck win frequency, possibly due to a tendency to preserve teammates' successful choices in a cooperative context to mitigate personal evaluation risks (Krieg and Xu, 2018; Ortiz et al., 2017).

3.3. Neural performance on the IGT

3.3.1. Inter-brain synchronization

A repeated measure ANOVA with the GROUP (COOP, COMP) as the between-participant factor and the STAGE (decision-making phase; feedback phase) as the within-participant factor was used on all channels across five FOIs to identify the group differences in the two decision phases. Given that significant differences were exclusively observed in FOI2 (0.340–0.381 Hz) and FOI4 (0.015–0.017 Hz), subsequent analyses focused specifically on these two frequencies of interest.

For FOI2 (0.340–0.381 Hz), the interaction effect of GROUP and STAGE at CH6 (BA9 - DLPFC) was significant, F (1, 58) = 12.358, FDR-corrected $p < 0.001$, $\eta_p^2 = 0.176$. A post hoc test with Bonferroni correction indicated that the IBS at CH6 for the decision-making stage was significantly higher than that for the feedback stage in the COMP group (FDR-corrected $p < 0.05$, see Fig. 10B and 10D). The main effects of GROUP and STAGE at CH6 were both not significant (for more details of statistical results see Table 4). In addition, the main effect of GROUP at CH12 (BA10 - FPC) was significant, F (1, 58) = 9.28, FDR-corrected $p < 0.01$, $\eta_p^2 = 0.138$. The post hoc test with Bonferroni correction indicated that the IBS for the COMP group was significantly higher than that

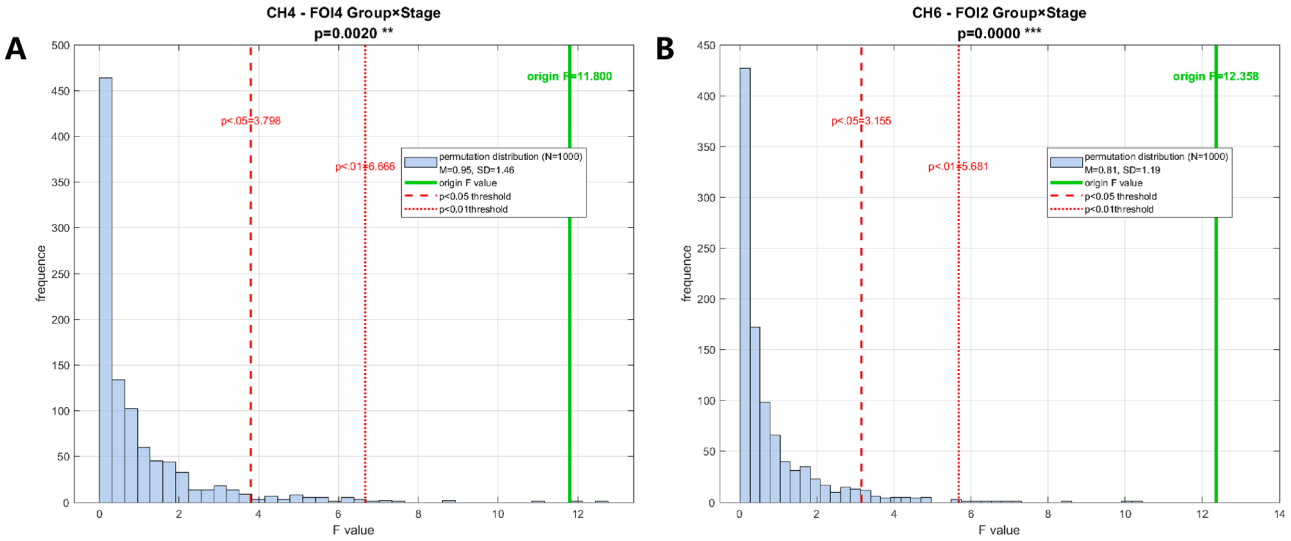

Fig. 11. Permutation test results of interaction main effect in CH4 and CH6. (A) Permutation test results of CH4 in FOI4. (B) Permutation test results of CH6 in FOI2. Here the green line represents the original F-value, while the light blue bars depict the distribution of F-values obtained from permutation testing. The two red dashed lines indicate the critical F-value thresholds at $p = 0.05$ and $p = 0.01$, respectively. The permutation test p-values are displayed below the chart title, accompanied by asterisk notations.

for the COOP group (FDR-corrected $p < 0.01$, see Fig. 9A). Moreover, the main effect of GROUP at CH20 (BA10 - FPC) was significant, F (1, 58) = 9.92, FDR-corrected $p < 0.01$, $\eta_p^2 = 0.146$. The post hoc test with Bonferroni correction indicated that the IBS for the COMP group was significantly higher than that for the COOP group (FDR-corrected $p <$ 0.01, see Fig. 9B). Similarly, the main effect of GROUP at CH21 (BA10 - FPC) was significant, F (1, 58) = 9.39, FDR-corrected $p < 0.01$, $\eta_p^2 =$ 0.139. The post hoc test with Bonferroni correction indicated that the IBS for the COMP group was significantly higher than that for the COOP group (FDR-corrected $p < 0.01$, see Fig. 9D), whereas the main effect of STAGE and the interaction effect at CH12, CH20, CH21 were all not significant (for more details of statistical result see Table 4).

For FOI4 (0.015–0.017 Hz), only the interaction effect of GROUP and STAGE at CH4 (BA9 - DLPFC) was significant, F (1, 58) = 11.80, FDR-corrected $p < 0.01$, $\eta_p^2 = 0.169$. The post hoc test with Bonferroni correction indicated that the IBS at CH4 for the decision-making stage was significantly higher than that for the feedback stage in the COMP group (FDR-corrected $p < 0.05$, see Fig. 10A and 10C). The main effect of GROUP and STAGE at CH4 were not significant (see more details in Table 4).

Furthermore, the interaction effect for CH6 at FOI2 ($p < 0.001$, see Fig. 11B), the main effect of group for CH12 at FOI2 ($p < 0.01$, see Fig. 12A), the main effect of group for CH20 at FOI2 ($p < 0.01$, see Fig. 12B), the main effect of group for CH21 at FOI2 ($p < 0.01$, see Fig. 12C), and the interaction effect for CH4 at FOI4 ($p < 0.01$, see Fig. 11A) all survived 1000 permutation tests. These results confirm that the findings of the present study reflect genuine experimental effects rather than random variation.

3.3.2. *Coupling directionality*

The GCA results found that the main effect of STAGE at CH4 (BA9 - DLPFC) was significant, F (1, 118) = 5.845, FDR-corrected $p < 0.05$, $\eta_p^2 =$ 0.047. A post hoc test with Bonferroni correction indicated that the GCA index in the decision-making stage was significantly higher than that in the feedback stage (FDR-corrected $p < 0.05$). In addition, the interaction effect of STAGE and DIRECTION at CH4 was also significant, F (1, 118) = 4.370, FDR-corrected $p < 0.05$, $\eta_p^2 = 0.036$. A post hoc test with Bonferroni correction indicated that the strength of the observer to decision-maker directed brain connections of dyads at the decision-making stage was significantly stronger than the decision-maker to observer directed brain connections of dyads at the feedback stage (FDR-corrected $p < 0.05$) in CH4 (see Fig. 13). No significant differences were observed in the other channels.

3.4. *The behavior-brain correlation*

Pearson correlation analysis was conducted to investigate the relationships among IBS, cognitive processes, and behavioral outcomes across different social contexts. As shown in Fig. 14C, in the cooperative (COOP) group, IBS at channel CH4 (BA9 - DLPFC) in FOI4 (0.015–0.017 Hz) during the decision-making stage ($r = 0.427$, $p < 0.05$) and the feedback stage ($r = 0.424$, $p < 0.05$) was positively correlated with IGT cumulative earnings. Additionally, IBS at channel CH20 (BA10-FPC) in FOI2 (0.340–0.381 Hz) during the decision-making stage ($r = -0.456$, $p < 0.05$) and the feedback stage ($r = -0.427$, $p < 0.05$) was negatively correlated with IGT net scores, as was IBS at channel CH21 (BA10-FPC) in FOI2 (0.340–0.381 Hz) ($r = -0.380$, $p < 0.05$ and $r = -0.408$, $p <$ 0.05, respectively).

As shown in Fig. 14B, in the competitive (COMP) group, reward sensitivity (α_{Rew}) was negatively correlated with IBS at CH21 (BA10-FPC) in FOI2 (0.340–0.381 Hz) during the decision-making stage ($r = -0.513$, $p < 0.01$) and the feedback stage ($r = -0.499$, $p < 0.01$) and with IGT cumulative earnings ($r = -0.447$, $p < 0.05$). Perseveration was negatively correlated with IGT net scores ($r = -0.374$, $p < 0.05$). In addition, the positive correlation between the IBS of the frontal pole (CH21 during feedback stage) and the weight parameter of selection persistence was marginally significant ($r = 0.344$, $p = 0.063$).

Across the 60 dyads, further significant correlations were observed. As shown in Fig. 14A, α_{Rew} was negatively associated with IBS at CH21 (BA10-FPC) in FOI2 (0.340–0.381 Hz) during both the decision-making stage ($r = -0.284$, $p < 0.05$) and the feedback stage ($r = -0.281$, $p <$ 0.05), indicating that higher reward sensitivity was linked to lower IBS. Accumulative earnings were positively associated with IBS at CH4 (BA9-DLPFC) in FOI4 (0.015–0.017 Hz) during the decision-making stage ($r =$ 0.296, $p < 0.05$) and the feedback stage ($r = 0.293$, $p < 0.05$), suggesting that greater IBS at CH4 was linked to higher earnings. Finally, net scores were negatively correlated with IBS at CH21 (BA10-FPC) in FOI2 (0.340–0.381 Hz) during the feedback stage ($r = -0.255$, $p < 0.05$), indicating that higher IBS at CH21 was associated with lower net scores.

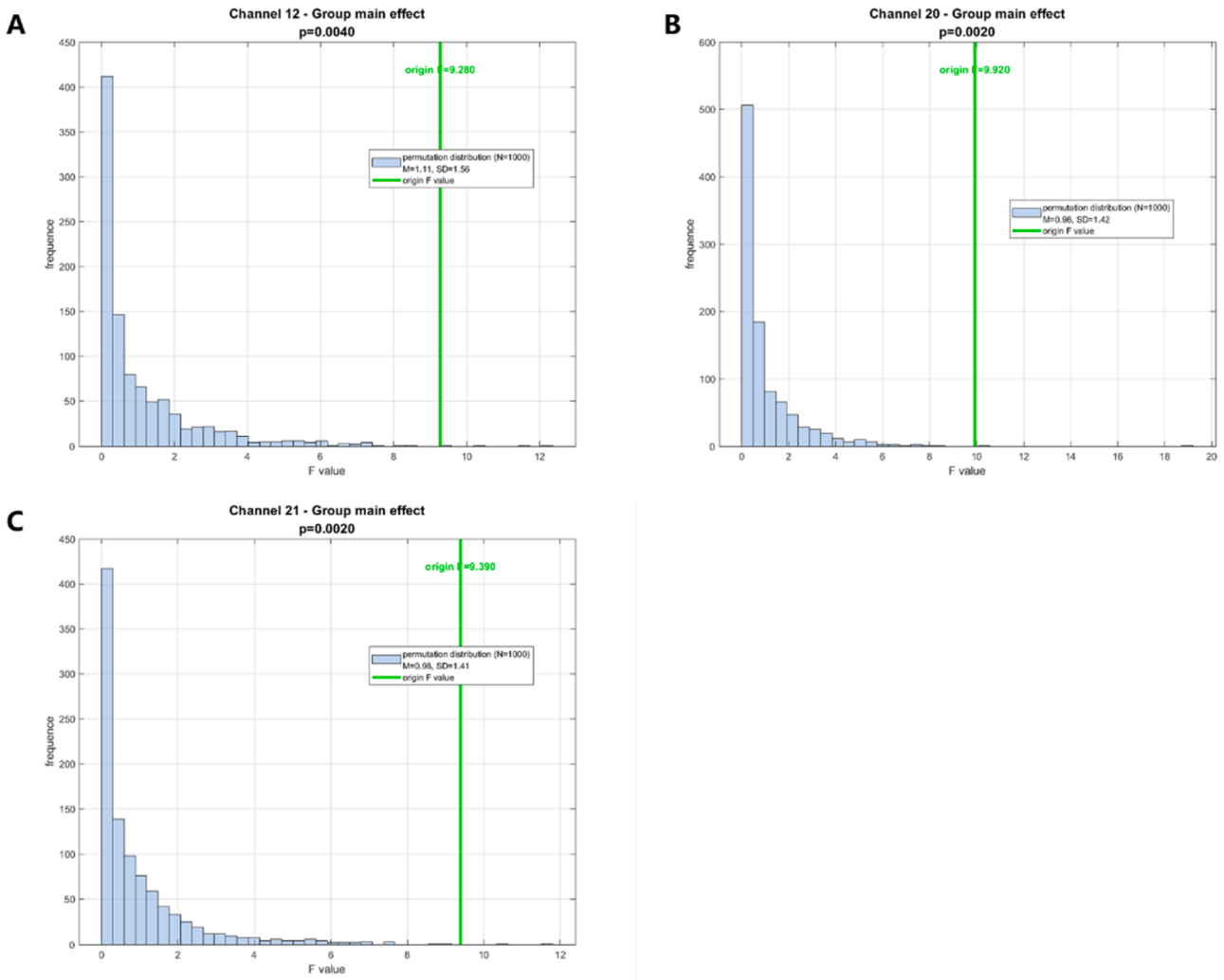

Fig. 12. Permutation test results of GROUP main effect in CH12, CH20, CH21 at FOI2. (A) Permutation test results of GROUP main effect in CH12. (B) Permutation test results of GROUP main effect in CH20. (C) Permutation test results of GROUP main effect in CH21. Here the green line represents the original F-value, while the light blue bars depict the distribution of F-values obtained from permutation testing. The permutation test p-values are displayed below the chart title.

4. Discussion

This study integrates RL modeling with dual-brain fNIRS hyperscanning to dissect the frequency-specific neural mechanisms and computational processes underlying cooperative and competitive dyadic risky decision-making. Behaviorally, competitive dyads achieved significantly higher cumulative earnings than cooperative dyads, whereas cooperators displayed a pronounced preference for high win-frequency choices, likely to mitigate social evaluation risks. Computational modeling revealed that the ORL model effectively captured this strategic divergence: cooperators exhibited elevated β_{fre} values (reward-frequency sensitivity), while competitors demonstrated more flexible, task-oriented strategies characterized by reduced reward sensitivity (α_{Rew}) and lower choice persistence.

The neuroimaging findings suggest a dual-pathway mechanism governing competitive dyadic interactions. We observed that FPC (BA10) synchronization in the mid-to-high frequency band (FOI2: 0.340–0.381 Hz) was intrinsically linked to opponent-focused monitoring and the inhibition of impulsive risk-seeking. Concurrently, DLPFC synchronization (BA9) in the ultra-low frequency band (FOI4: 0.015–0.017 Hz) correlated with generalized cognitive control and enhanced decision efficiency. This frequency-specific functional mapping aligns with our RL-based behavioral inferences and converges with prior hyperscanning work (Peng et al., 2025), which reported context-dependent modulation of IBS in cooperative versus competitive decision-making. Importantly, our approach extends this literature by resolving the spectral architecture of these effects and linking discrete frequencies to specific latent cognitive parameters.

4.1. *Prefrontal synchronization in competition: A dual-pathway framework for risk decision-making*

Our findings support and refine the context-specific neural coupling effects observed by Peng et al. (2025), who demonstrated increased IBS in competitive interactions within prefrontal regions. In the present study, we show that these enhancements are not homogeneous: FPC IBS in FOI2 is associated with greater opponent monitoring (positively correlated with β_{pers}) and reduced reward-driven learning processes (negatively correlated with α_{Rew}, which is associated with reduced cumulative earnings), while DLPFC IBS in FOI4 is positively correlated with cumulative earnings, reflecting sustained goal-directed control. This specialization suggests that competitive advantage emerges from a division of labor between fast social information processing and slower, strategic cognitive control—a pattern consistent with the DLPFC's established role in orchestrating goal-oriented behavior (Miller and Cohen, 2001) and with the coordination–efficiency trade-offs outlined

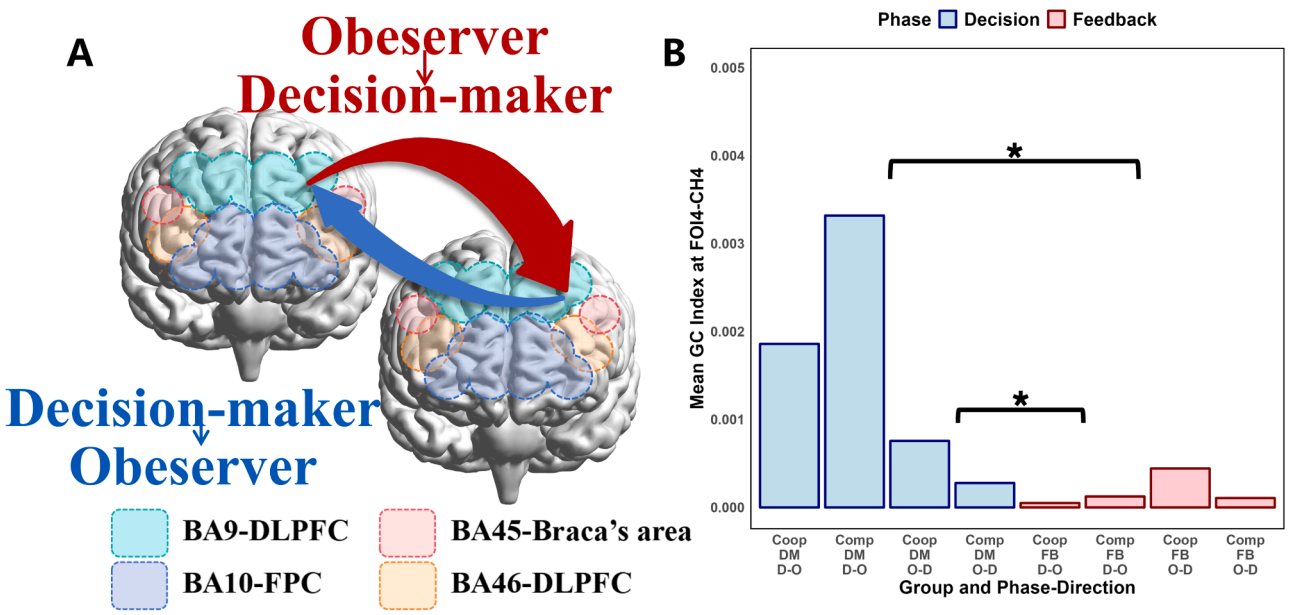

Fig. 13. Directional coupling (Granger causality analysis) in CH4 (BA9, DLPFC).
(A) Schematic illustration of the GCA results. The red arrow indicates the direction of coupling from the observer to the decision-maker, while the blue arrow indicates the direction from the decision-maker to the observer. The thickness of the arrow and the height of the bars represent the coupling strength. (B) Bar plot of the ANOVA results. A significant main effect of STAGE was observed: GCA indices were significantly higher during the decision-making stage than during the feedback stage (FDR-corrected $p < 0.05$). Furthermore, a significant STAGE × DIRECTION interaction was found: the observer-to-decision-maker coupling strength during the decision-making stage was significantly stronger than the decision-maker-to-observer coupling strength during the feedback stage (FDR-corrected $p < 0.05$). The asterisk (*) denotes significance at an FDR-corrected $p < 0.05$.

in Peng et al. (2025). This dual pathway architecture, in which ultra-low frequency DLPFC coupling supports decision efficiency and higher frequency FPC coupling supports social monitoring, provides a mechanistic account of competitive advantage and outlines directions for future research. As these frequency ranges were identified through exploratory analyses in a single cohort, their functional interpretation remains preliminary. Whether FOI4 and FOI2 selectively index social monitoring or cognitive control requires replication in independent samples and direct comparison with hyperscanning studies using comparable spectral definitions. Future work will combine multi-site recordings, cross frequency coupling analyses, and causal perturbation approaches such as transcranial direct current stimulation to test and refine the proposed mapping between frequency and function.

4.2. *The ORL model as a bridge between cognitive algorithms and neural coupling*

The ORL framework outperformed alternative RL models (e.g., PVL_delta) by dissociating gain and loss learning rates (α_{Rew}, α_{Pun}) and quantifying win-frequency weighting (β_{fre}). Elevated β_{fre} values in cooperative dyads indicate a bias toward probabilistic safety, whereas lower β_{fre} in competitive dyads reflects more dynamic value tracking that is less tied to immediate reward probability, a pattern consistent with adaptive optimization in competitive contexts. Our findings further suggest that these computational differences are grounded in prefrontal synchronization. The positive association between ultra-low frequency DLPFC coupling (FOI4) and cumulative earnings indicates that synchronized activity supports stable goal directed reward learning processes indexed by the decrease of α_{Rew}. In contrast, mid to high frequency FPC synchronization (FOI2) appears to support the integration of social contextual cues, which may account for the stronger influence of win frequency (β_{fre}) in cooperative contexts. By linking FOI-specific IBS with RL parameters, this study provides a mechanistic account of how coordinated prefrontal activity supports adaptive decision making across social contexts, extending prior work (Peng et al., 2025) that has focused on broader frequency ranges.

4.3. *Cooperative reward–win frequency bias: Neural costs of social alignment*

Beyond the computational mechanisms, the preference of cooperative dyads for high reward-frequency options despite lower earnings reflects a significant social-behavioral trade-off. This pattern is consistent with the diffusion of responsibility described by Darley and Latane (1968), where shared risk reduces individual accountability and promotes choices that appear safer but are suboptimal (Peng et al. 2025). At the neural level, the FPC synchronization (BA 10) in the FOI2 band, which is associated with this behavioral bias, suggests that cooperation shifts cognitive resources away from analytical risk evaluation toward the maintenance of shared intentionality (Pan et al., 2017). By integrating environmental information and promoting social alignment, the FPC highlights a key trade off in which cooperation favors relational stability at the cost of reward optimization. These findings link behavioral inefficiency with increased neural synchrony and provide a mechanistic account of how socially driven motivations shape the neural basis of decision making.

4.4. *Theoretical and practical implication*

This study advances a dual-system framework combining neural mechanisms with computational processes to reveal how social contexts reshape prefrontal dynamics in adaptive decision-making. By integrating dual-brain fNIRS hyperscanning with reinforcement learning modeling, we reveal frequency-specific mechanisms through which competition and cooperation engender a tradeoff between strategic efficiency and social cohesion. In competitive environments, dual brain synchronization of FOI2 in the FPC reduce reward-driven risk-seeking strategies by focusing on social information, a process indexed by heightened IBS in decision-critical channels (CH12/CH20/CH21). In addition, neural coupling of FOI4 in the DLPFC may represent task-

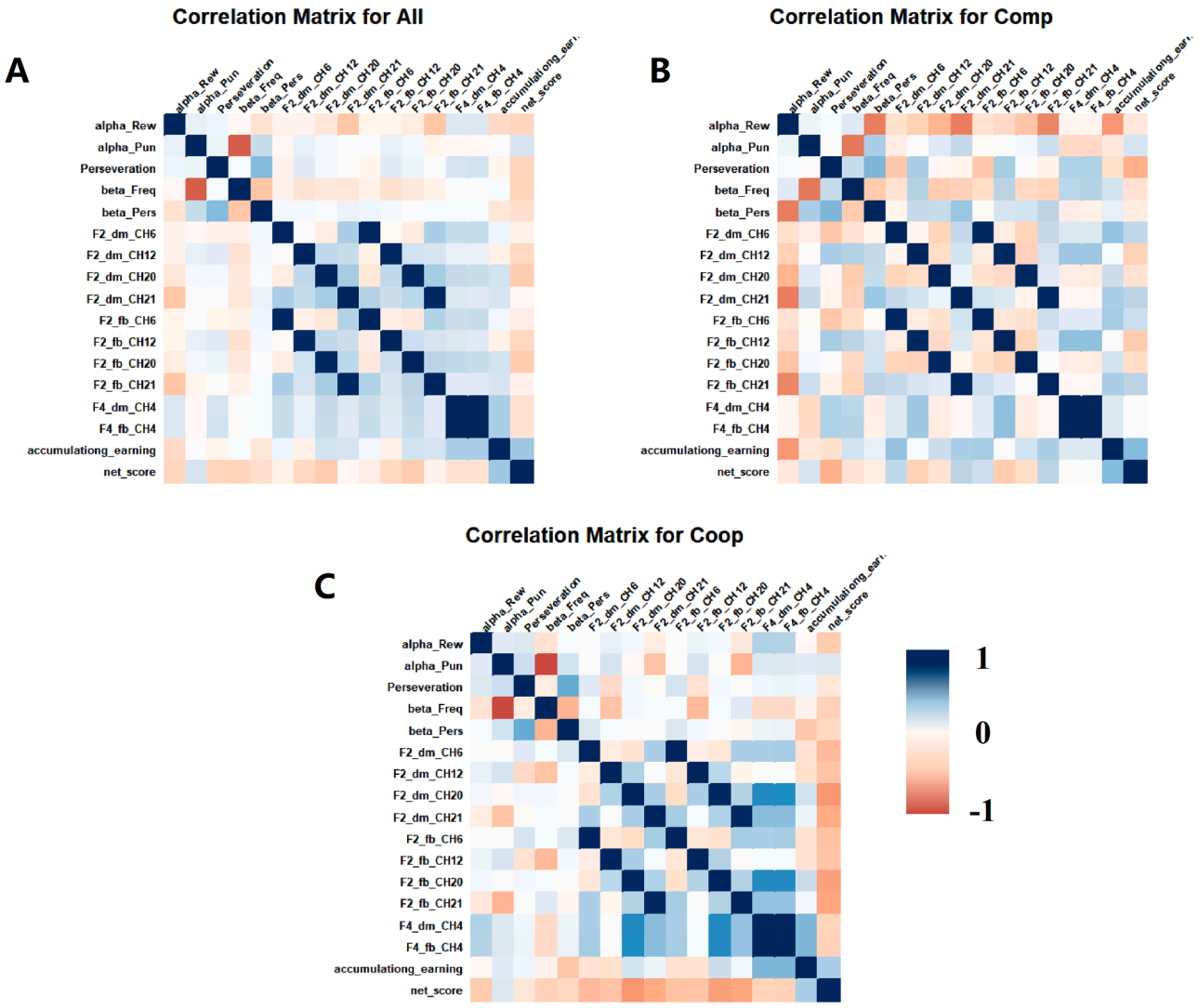

Fig. 14. Correlations between IBS, RL parameters, and behavioral performance. (A) All dyads: α_{Rew} was negatively associated with IBS at CH21 (FOI2) during both stages ($p < 0.05$). Accumulative earnings positively correlated with IBS at CH4 (FOI4) in both stages ($p < 0.05$). Net scores negatively correlated with IBS at CH21 (FOI2) during feedback ($p < 0.05$). (B) COMP group: α_{Rew} negatively correlated with IBS at CH21 (FOI2) in both stages ($p < 0.05$) and with accumulative earnings ($p < 0.05$). Perseveration negatively correlated with net scores ($p < 0.05$). A marginally significant positive correlation was found between frontal pole IBS (CH21 during feedback stage) and selection persistence weight ($p = 0.06$). (C) COOP group: IBS at CH4 (FOI4) during both decision-making and feedback positively correlated with cumulative earnings ($p < 0.05$). IBS at CH20 and CH21 (FOI2) during both stages negatively correlated with net scores ($p < 0.05$).

general cognitive control, aligning with the DLPFC's role in sustaining goal-directed control through large-scale cortical integration (Miller and Cohen, 2001). Conversely, cooperation shows reduced IBS in the FPC, reflecting responsibility diffusion—a state where teammate presence attenuates decision-relevant information extraction, as per the coordination-efficiency trade-off.

These findings clarify the competition-cooperation paradox. In competition, participants simultaneously monitor task cues and the opponent, which supports strategic dominance. In cooperation, they trade analytical precision for relational stability, leading to responsibility diffusion. By linking prefrontal oscillatory coupling (lower vs. higher IBS) to context-specific learning, we connect social neuroscience with computational psychiatry. The ORL model captures this dissociation. Higher β_{fre} in cooperative contexts reflects a cautious bias driven by synchronized rhythms, whereas competitive contexts favor rapid value updating that is less dependent on immediate reward probability (Haines et al., 2018). In this way, social context constrains reinforcement learning processes and helps reconcile differing accounts of social risk taking (Linde and Sonnemans, 2015).

Practically, these insights offer actionable biomarkers for both clinical and technological applications. DLPFC-IBS could guide interventions for disorders characterized by social-cognitive inflexibility (e.g., autism spectrum disorder), where impaired strategic filtering exacerbates social interference. Conversely, the negative correlation between frontopolar IBS and task efficiency identifies synchronization thresholds for optimizing cooperative systems—insights applicable to neurofeedback protocols requiring balanced social-task coordination. For instance, modulating frontopolar hyper-synchronization via real-time fNIRS feedback might enhance cooperative decision-making without sacrificing relational harmony.

4.5. *Limitations and future prospects*

Despite the insights gained, several limitations of the present study warrant acknowledgment. First, the recruitment of an exclusively female sample, while intentional to control for gender-related variability in social cognition (Wang and Li, 2024), restricts the generalizability of our findings. Given documented gender differences in the neural dynamics of competition and social decision-making (Liu et al., 2020), future research should employ balanced or mixed-gender dyads to

enhance the ecological validity of the results. Second, our neural measurements were restricted to frontal regions due to equipment-related spatial constraints. Whilst the prefrontal cortex is a critical hub for reinforcement learning and strategic control, social decision-making typically engages a distributed "social brain" network, including the temporo-parietal junction (TPJ) and superior temporal sulcus (STS), which are implicated in mentalizing and intention attribution (Hu et al., 2025; Lu et al., 2020b; Wang et al., 2024). Future hyperscanning investigations should adopt whole-head montages or multi-site probe arrays to delineate the coordination between these posterior regions and frontal oscillatory dynamics. Third, although our computationally intensive trial-shuffling permutation analysis confirmed the robustness of the identified IBS effects, the 1-minute resting-state baseline employed remains relatively brief. Future studies might consider longer baseline recordings or the inclusion of diverse control conditions (e.g., non-interactive tasks) to further isolate task-specific inter-brain coupling. Fourth, the computational modeling approach treated each dyad as a single decision-making agent. Alhough this abstraction offers a parsimonious framework that aligns naturally with inter-brain synchrony metrics and facilitates modeling of supra-individual dynamics (Blanchard et al., 2025; Li et al., 2024), it inevitably sacrifices granularity in capturing the bidirectional observation and adaptation processes that occur within dyadic interactions. Future "social reinforcement learning" models could overcome this limitation by incorporating interpersonal prediction-error signals, potentially indexed by dorsolateral prefrontal inter-brain synchrony or specific frequency bands (e.g., FOI2). Finally, although the IGT is a well-established paradigm for studying risky choices, it abstracts away from the complexities of real-world social risks. Subsequent research should examine whether the frequency-specific mechanisms identified here generalize to high-stakes, ecologically valid paradigms, such as iterative economic bargaining or complex cooperative-competitive games with tangible social outcomes.

Funding

This research was supported in part by the National Natural Science Foundation of China (72171151, 72571180), the Fundamental Research Funds for the Central Universities (41005234) and the Academic Mentoring Program of Shanghai International Studies University (2025DSYL051).

Compliance with ethical standards

The current study complied with the Declaration of Helsinki, and was authorized by the Institutional Review Board of the Academic Committee of Key Laboratory of Brain-Machine Intelligence for Information Behavior at Shanghai International Studies University in China.

Data and code availability statement

Due to the requirements and regulations of the Key Laboratory of Brain-Machine Intelligence for Information Behavior at Shanghai International Studies University in China, the data and code that supported the present study are available from the corresponding author upon reasonable request with the approval from the Institutional Review Board of the Key Laboratory of Brain-Machine Intelligence for Information Behavior at Shanghai International Studies University in China.

CRediT authorship contribution statement

Mingjing Wang: Writing – original draft, Formal analysis, Data curation. **Sihua Xu:** Writing – review & editing, Writing – original draft, Supervision, Investigation, Funding acquisition, Conceptualization. **Linden J. Ball:** Writing – review & editing.

Declaration of competing interest

The authors declare that the research was conducted in the absence of any commercial or financial relationships that could be construed as a potential conflict of interest.

Supplementary materials

Supplementary material associated with this article can be found, in the online version, at doi:10.1016/j.neuroimage.2026.121942.

References

Alibakhshi, A., Hartke, B., 2021. Improved prediction of solvation free energies by machine-learning polarizable continuum solvation model. Nat. Commun. 12 (1), 3584. https://doi.org/10.1038/s41467-021-23724-6.

Arnold, L., Völkel, M., Rosendahl, J., Rost, M., 2025. A multi-level meta-analysis of the relationship between decision-making during birth and postpartum mental health. Health psychol. behav. med. 13 (1). https://doi.org/10.1080/21642850.2025.2456032.

Baker, J.M., Liu, N., Cui, X., Vrticka, P., Saggar, M., Hosseini, S.M.H., Reiss, A.L., 2016. Sex differences in neural and behavioral signatures of cooperation revealed by fNIRS hyperscanning. Sci. Rep. 6 (1), 26492. https://doi.org/10.1038/srep26492.

Blanchard, M.D., Aidman, E., Stankov, L., Kleitman, S., 2025. A recipe for dyadic collective intelligence for well-structured tasks: mix equal parts cognitive ability and confidence plus a pinch of social sensitivity. Cogn. Res. Princ. Implic. 10 (1), 63. https://doi.org/10.1186/s41235-025-00655-0.

Bogacz, R., 2017. A tutorial on the free-energy framework for modelling perception and learning. J. Math. Psychol. 76, 198–211. https://doi.org/10.1016/j.jmp.2015.11.003.

Bressler, S.L., Seth, A.K., 2011. Wiener-Granger Causality: A well established methodology. NeuroImage 58 (2), 323–329. https://doi.org/10.1016/j.neuroimage.2010.02.059.

Buckley, C.L., Kim, C.S., McGregor, S., Seth, A.K., 2017. The free energy principle for action and perception: A mathematical review. J. Math. Psychol. 81, 55–79. https://doi.org/10.1016/j.jmp.2017.09.004.

Bulgarelli, C., et al., 2018. Dynamic causal modelling on infant fNIRS data: A validation study on a simultaneously recorded fNIRS-fMRI dataset. NeuroImage 175, 413–424. https://doi.org/10.1016/j.neuroimage.2018.04.022.

Chen, M., et al., 2020. Neural alignment during face-to-face spontaneous deception: Does gender make a difference? Hum. Brain Mapp. 41 (17), 4964–4981. https://doi.org/10.1002/hbm.25173.

Chen, F., et al., 2021. Abnormal negative feedback processing in individuals with autistic traits in the Iowa gambling task: Evidence from behavior and event-related potentials. Int. J. Psychophysiol. 165, 36–46. https://doi.org/10.1016/j.ijpsycho.2021.02.018.

Chen, L., et al., 2022. The increased inter-brain neural synchronization in prefrontal cortex between simulated patient and acupuncturist during acupuncture stimulation: Evidence from functional near-infrared spectroscopy hyperscanning. Hum. Brain Mapp. 44 (3), 980–988. https://doi.org/10.1002/hbm.26120.

Cheng, X.J., Liu, M.H., Pan, Y.F., 2022. Shared responsibility promotes the benefit of interactive decision- making in novices: A hyperscanning study. Acta Psychol. Sin. 54 (11), 1391–1402. https://doi.org/10.3724/SP.J.1041.2022.01391.

Cooper, D.A., 2024. Diffusion of Responsibility for Actions With Advice. J. Behav. Decis. Mak. 37 (4). https://doi.org/10.1002/bdm.2415.

Cui, X., Bryant, D.M., Reiss, A.L., 2012. NIRS-based hyperscanning reveals increased interpersonal coherence in superior frontal cortex during cooperation. NeuroImage 59 (3), 2430–2437. https://doi.org/10.1016/j.neuroimage.2011.09.003.

Darley, J.M. and Latane, B. 1968. Bystander intervention in emergencies: Diffusion of responsibility. J. Pers. Soc. Psychol. 8(4, Pt.1), pp. 377–383. doi:10.1037/h0025589.

Daunizeau, J., Ligneul, R., 2019. Sequential exploration in the Iowa gambling task: Validation of a new computational model in a large dataset of young and old healthy participants. PLoS Comput. Biol. 15 (6). https://doi.org/10.1371/journal.pcbi.1006989.

Fareri, D.S., Delgado, M.R., 2014. Differential reward responses during competition against in- and out-of-network others. Soc. Cogn. Affect. Neurosci. 9 (4), 412–420. https://doi.org/10.1093/scan/nst006.

Faul, F., Erdfelder, E., Lang, A.G., Buchner, A., 2007. G*Power 3: a flexible statistical power analysis program for the social, behavioral, and biomedical sciences. Behav. Res. Methods 39 (2), 175–191. https://doi.org/10.3758/bf03193146.

FeldmanHall, O., Shenhav, A., 2019. Resolving uncertainty in a social world. Nat. Hum. Behav. 3 (5), 426–435. https://doi.org/10.1038/s41562-019-0590-x.

Feng, X., Xu, X., Meng, Z., Jiang, J., Pei, M., Zheng, Y., Lu, C., 2025. A rapid cortical learning process supporting students' knowledge construction during real classroom teaching. Adv. Sci. (Weinh) 12 (18), e2416610. https://doi.org/10.1002/advs.202416610.

Fliessbach, K., Weber, B., Trautner, P., Dohmen, T., Sunde, U., Elger, C.E., Falk, A., 2007. Social comparison affects reward-related brain activity in the human ventral striatum. Science 318 (5854), 1305–1308. https://doi.org/10.1126/science.1145876.

Frith, C.D., Frith, U., 2012. Mechanisms of social cognition. Annu. Rev. Psychol. 63, 287–313. https://doi.org/10.1146/annurev-psych-120710-100449.

Fukushima, Y., Yoshidome, T., 2023. A deep-learning model for grid-based solvation free energy. Biophys. J. 122 (3), 141A–142A. https://doi.org/10.1016/j.bpj.2022.11.926.
Gärling, T., Fang, D., Holmen, M., Michaelsen, P., 2020. Financial risk-taking related to individual risk preference, social comparison and competition. Rev. Behav. Finance 13 (2), 125–140. https://doi.org/10.1108/rbf-11-2019-0153.
Granger, C.W.J., 1969. Investigating causal relations by econometric models and cross-spectral methods. Econometrica 37 (3), 424–438. https://doi.org/10.2307/1912791.
Grinsted, A., Moore, J.C., Jevrejeva, S., 2004. Application of the cross wavelet transform and wavelet coherence to geophysical time series. Nonlinear. Process. Geophys 11 (5–6), 561–566. https://doi.org/10.5194/npg-11-561-2004.
Guglielmini, S., Bopp, G., Marcar, V.L., Scholkmann, F., Wolf, M., 2022. Cross-Frequency coupling between brain and body biosignals: A systemic physiology augmented functional near-infrared spectroscopy hyperscanning study. Adv. Exp. Med. Biol. 1395, 171–176. https://doi.org/10.1007/978-3-031-14190-4_29.
Haines, N., Vassileva, J., Ahn, W., 2018. The outcome-representation learning model: A novel reinforcement learning model of the Iowa gambling task. Cogn. Sci. 42 (8), 2534–2561. https://doi.org/10.1111/cogs.12688.
Horn, S., Freund, A.M., 2021. Adult age differences in monetary decisions with real and hypothetical reward. J. Behav. Decis. Mak. 35 (2). https://doi.org/10.1002/bdm.2253.
Hou, Y., Song, B., Hu, Y., Pan, Y., Hu, Y., 2020. The averaged inter-brain coherence between the audience and a violinist predicts the popularity of violin performance. NeuroImage 211. https://doi.org/10.1016/j.neuroimage.2020.116655.
Hou, Y., Zhang, D., Gan, X., Hu, Y., 2022. Group polarization calls for group-level brain communication. NeuroImage 264. https://doi.org/10.1016/j.neuroimage.2022.119739.
Hu, Y., Zhang, R., Duan, Z., Liu, M., Cheng, X., 2025. Unequal allocation alters the benefit of interactive decision-making in novices: A hyperscanning study. NeuroImage 319, 121430. https://doi.org/10.1016/j.neuroimage.2025.121430.
Huang, G.H., Shi, Q.H., Zheng, S., Zhao, K., Fu, X.L., 2025. Sense of Self-Agency and Other-Agency Under Social Interaction Contexts. Int. J. Hum.-Comput. Int. 41 (9), 5373–5383. https://doi.org/10.1080/10447318.2024.2359749.
Im, C.H., Jung, Y.J., Lee, S., Koh, D., Kim, D.W., Kim, B.M., 2010. Estimation of directional coupling between cortical areas using Near-Infrared Spectroscopy (NIRS). Opt. Express 18 (6), 5730–5739. https://doi.org/10.1364/OE.18.005730.
Jiang, J., Chen, C., Dai, B., Shi, G., Ding, G., Liu, L., Lu, C., 2015. Leader emergence through interpersonal neural synchronization. Proc. Natl. Acad. Sci. 112 (14), 4274–4279. https://doi.org/10.1073/pnas.1422930112.
Jin, Z., Yin, J., Pan, Y., Zhang, Y., Li, Y., Xu, X., Luo, J., 2024. Teach a man to fish: hyper-brain evidence on scaffolding strategy enhancing creativity acquisition and transfer. NeuroImage 297. https://doi.org/10.1016/j.neuroimage.2024.120757.
Jones, R.M., et al., 2011. Behavioral and neural properties of social reinforcement learning. J. Neurosci. 31 (37), 13039–13045. https://doi.org/10.1523/JNEUROSCI.2972-11.2011.
Junyi, D.A.I., Yue, S., Xinyun, H.U., 2023. Strategy switching in a sequence of decisions: Evidence from the Iowa Gambling Task. Acta Psychol. Sin. 55 (11). https://doi.org/10.3724/sp.J.1041.2023.01793.
Knyazev, G.G., Savostyanov, A.N., Bocharov, A. v, Rudych, P.D. and Saprigyn, A.E. 2024. Multivariate pattern analysis of cooperation and competition in constructive action. Neuropsychologia 202. doi:10.1016/j.neuropsychologia.2024.108956.
Krieg, A., Xu, Y.Y., 2018. From self-construal to threat appraisal: understanding cultural differences in social anxiety between Asian Americans and European Americans. Cultur. Divers. Ethnic Minor. Psychol. 24 (4), 477–488. https://doi.org/10.1037/cdp0000194.
Kumar, R., Janakiprasad Kumar, Benegal, V., 2019. Underlying decision making processes on Iowa Gambling Task. Asian J. Psychiatr. 39, 63–69. https://doi.org/10.1016/j.ajp.2018.12.006.
León, J.J., et al., 2023. Decision-making and frontoparietal resting-state functional connectivity among impulsive-compulsive diagnoses. Insights from a Bayesian approach. Addict. Behav. 143. https://doi.org/10.1016/j.addbeh.2023.107683.
Li, S., Yu, L., Gan, X., Hou, Y., Pan, Y., Luo, Y., Hu, Y., 2024. The acquired dyad inclination and decreased interpersonal brain communication in the pursuit of collective benefit. NeuroImage 297. https://doi.org/10.1016/j.neuroimage.2024.120700.
Li, Y., et al., 2019. Hemispheric mPFC asymmetry in decision making under ambiguity and risk: An fNIRS study. Behav. Brain Res. 359, 657–663. https://doi.org/10.1016/j.bbr.2018.09.021.
Liang, Z., Li, S., Zhou, S., Chen, S., Li, Y., Chen, Y., Zhou, Z., 2022. Increased or decreased? Interpersonal neural synchronization in group creation. NeuroImage 260. https://doi.org/10.1016/j.neuroimage.2022.119448.
Linde, J., Sonnemans, J., 2015. Decisions under risk in a social and individual context: The limits of social preferences. J. Behav. Exp. Econ. 56, 62–71. https://doi.org/10.1016/j.socec.2015.03.003.
Liu, Z., Liu, T., Mu, S., 2020. Gender differences in the effects of competition and cooperation on risk-taking under ambiguity. PsyCh J 10 (3), 374–383. https://doi.org/10.1002/pchj.419.
Liu, Q., et al., 2023. Inter-brain neural mechanism and influencing factors underlying different cooperative behaviors: a hyperscanning study. Brain Struct. Funct. 229 (1), 75–95. https://doi.org/10.1007/s00429-023-02700-4.
Lockwood, P.L., Wittmann, M.K., Apps, M.A.J., Klein-Flügge, M.C., Crockett, M.J., Humphreys, G.W., Rushworth, M.F.S., 2018. Neural mechanisms for learning self and other ownership. Nat. Commun. 9 (1). https://doi.org/10.1038/s41467-018-07231-9.
Lu, K., Teng, J., Hao, N., 2020a. Gender of partner affects the interaction pattern during group creative idea generation. Exp. Brain Res. 238 (5), 1157–1168. https://doi.org/10.1007/s00221-020-05799-7.
Lu, K., Yu, T., Hao, N., 2020b. Creating while taking turns, the choice to unlocking group creative potential. Neuroimage 219. https://doi.org/10.1016/j.neuroimage.2020.117025.
Lu, H., Wang, X., Zhang, Y., Huang, P., Xing, C., Zhang, M., Zhu, X., 2023. Increased interbrain synchronization and neural efficiency of the frontal cortex to enhance human coordinative behavior: A combined hyper-tES and fNIRS study. NeuroImage 282. https://doi.org/10.1016/j.neuroimage.2023.120385.
Lv, J.C., Liu, J.S., 2014. Model selection principles in misspecified models. J. R. Stat. Soc. Ser. B Stat. Methodol. 76 (1), 141–167. https://doi.org/10.1111/rssb.12023.
Miller, E.K., Cohen, J.D., 2001. An integrative theory of prefrontal cortex function. Annu. Rev. Neurosci. 24, 167–202. https://doi.org/10.1146/annurev.neuro.24.1.167.
Morel, P., 2018. Gramm: grammar of graphics plotting in Matlab. J. Open Source Softw. 3 (23), 568. https://doi.org/10.21105/joss.00568.
Nejati, V., Peyvandi, A., Nazari, N., Dehghan, M., 2024. Cognitive correlates of risky decision-making in individuals with and without ADHD: A meta-analysis. Neuropsychol. Rev. https://doi.org/10.1007/s11065-024-09646-2.
Nguyen, T., Hoehl, S., Vrtička, P., 2021. A guide to parent-child fNIRS hyperscanning data processing and analysis. Sensors 21 (12), 4075. https://doi.org/10.3390/s21124075.
Niso, G., Bruna, R., Pereda, E., Gutierrez, R., Bajo, R., Maestu, F., del-Pozo, F., 2013. HERMES: towards an integrated toolbox to characterize functional and effective brain connectivity. Neuroinformatics 11 (4), 405–434. https://doi.org/10.1007/s12021-013-9186-1.
Nozawa, T., Sasaki, Y., Sakaki, K., Yokoyama, R., Kawashima, R., 2016. Interpersonal frontopolar neural synchronization in group communication: An exploration toward fNIRS hyperscanning of natural interactions. NeuroImage 133, 484–497. https://doi.org/10.1016/j.neuroimage.2016.03.059.
Ortiz, J., Chang, S.H., Chih, W.H., Wang, C.H., 2017. The contradiction between self-protection and self-presentation on knowledge sharing behavior. Comput. Hum. Behav. 76, 406–416. https://doi.org/10.1016/j.chb.2017.07.031.
Palminteri, S., Wyart, V., Koechlin, E., 2017. The Importance of Falsification in Computational Cognitive Modeling. Trends Cogn. Sci. 21 (6), 425–433. https://doi.org/10.1016/j.tics.2017.03.011.
Pan, Y., Cheng, X., Zhang, Z., Li, X., Hu, Y., 2017. Cooperation in lovers: An fNIRS-based hyperscanning study. Hum. Brain Mapp. 38 (2), 831–841. https://doi.org/10.1002/hbm.23421.
Park, J., Shin, J., Lee, J., Jeong, J., 2023. Inter-Brain Synchrony Pattern Investigation on Triadic Board Game Play-Based Social Interaction: An fNIRS Study. IEEE Trans. Neural Syst. Rehabil. Eng. 31, 2923–2932. https://doi.org/10.1109/TNSRE.2023.3292844.
Peng, M., Yang, X., Cai, H., Cai, M., Li, X. and Zhang, M. 2025. Learn from your competitor or cooperator? A hyperscanning functional near-infrared spectroscopy study of gender-specific neural dynamics during interactive learning. 35(7). doi:10.1093/cercor/bhaf196.
Prlic, A., Daunizeau, J., Adam, V., Rigoux, L., 2014. VBA: A probabilistic treatment of nonlinear models for neurobiological and behavioural data. PLOS Computa. Bio. 10 (1), e1003441. https://doi.org/10.1371/journal.pcbi.1003441.
Reale, C., et al., 2023. Decision-making during high-risk events: A systematic literature review. J. Cogn. Eng. Decis. Mak. 17 (2), 188–212. https://doi.org/10.1177/15553434221147415.
Reindl, V., Gerloff, C., Scharke, W., Konrad, K., 2018. Brain-to-brain synchrony in parent-child dyads and the relationship with emotion regulation revealed by fNIRS-based hyperscanning. NeuroImage 178, 493–502. https://doi.org/10.1016/j.neuroimage.2018.05.060.
Rieger, S., Klee, S., Baumgarten, D., 2018. Experimental characterization and correlation of mayer waves in retinal vessel diameter and arterial blood pressure. Front. Physiol. 9. https://doi.org/10.3389/fphys.2018.00892.
Roos, Y., Krämer, M.D., Richter, D., Wrzus, C., 2024. Persons in contexts: The role of social networks and social density for the dynamic regulation of Face-to-Face interactions in daily life. J. Pers. Soc. Psychol. 127 (4), 920–935. https://doi.org/10.1037/pspp0000512.
Ruff, C.C., Fehr, E., 2014. The neurobiology of rewards and values in social decision making. Nat. Rev. Neurosci. 15 (8), 549–562. https://doi.org/10.1038/nrn3776.
Schmitz, F., Kunina-Habenicht, O., Hildebrandt, A., Oberauer, K., Wilhelm, O., 2018. Psychometrics of the Iowa and berlin gambling tasks: Unresolved issues with reliability and validity for risk taking. Assessment 27 (2), 232–245. https://doi.org/10.1177/1073191117750470.
Scholkmann, F., Kleiser, S., Metz, A.J., Zimmermann, R., Mata Pavia, J., Wolf, U., Wolf, M., 2014. A review on continuous wave functional near-infrared spectroscopy and imaging instrumentation and methodology. NeuroImage 85, 6–27. https://doi.org/10.1016/j.neuroimage.2013.05.004.
Schulze, C., Newell, B.R., 2015. Compete, coordinate, and cooperate: How to exploit uncertain environments with social interaction. J. Exp. Psychol. Gen. 144 (5), 967–981. https://doi.org/10.1037/xge0000096.
Song, X., Dong, M., Feng, K., Li, J., Hu, X., Liu, T., 2024. Influence of interpersonal distance on collaborative performance in the joint Simon task—An fNIRS-based hyperscanning study. NeuroImage 285. https://doi.org/10.1016/j.neuroimage.2023.120473.
Spektor, M.S., Kellen, D., 2018. The relative merit of empirical priors in non-identifiable and sloppy models: Applications to models of learning and decision-making. Psychon. Bull. Rev. 25 (6), 2047–2068. https://doi.org/10.3758/s13423-018-1446-5.

Steingroever, H., Wetzels, R., Wagenmakers, E.-J., 2016. Bayes factors for reinforcement-learning models of the Iowa gambling task. Decision 3 (2), 115–131. https://doi.org/10.1037/dec0000040.

Steingroever, H., Pachur, T., Smíra, M., Lee, M.D., 2018. Bayesian techniques for analyzing group differences in the Iowa Gambling Task: A case study of intuitive and deliberate decision-makers. Psychon. Bull. Rev. 25 (3), 951–970. https://doi.org/10.3758/s13423-017-1331-7.

Stephan, K.E., Penny, W.D., Daunizeau, J., Moran, R.J., Friston, K.J., 2009. Bayesian model selection for group studies. NeuroImage 46 (4), 1004–1017. https://doi.org/10.1016/j.neuroimage.2009.03.025.

Stolle, C.M., Gula, B., Yu, R.J., Huang, Y., 2024. The impact of diversity on group decision-making in the face of the free-rider problem. Judgm. Decis. Mak. 19. https://doi.org/10.1017/jdm.2023.47.

Sun, B., Xiao, W., Lin, S., Shao, Y., Li, W., Zhang, W., 2021. Cooperation with partners of differing social experience: An fNIRS-based hyperscanning study. Brain Cogn 154, 105803. https://doi.org/10.1016/j.bandc.2021.105803.

Suzuki, S., O'Doherty, J.P., 2020. Breaking human social decision making into multiple components and then putting them together again. Cortex 127, 221–230. https://doi.org/10.1016/j.cortex.2020.02.014.

Takada, T., Kono, M., Yokomitsu, K., 2023. Does Cooperation with Others Reduce Risky Gambling Behavior. Japan Psych. Res. https://doi.org/10.1111/jpr.12475.

Tang, H., Mai, X., Wang, S., Zhu, C., Krueger, F., Liu, C., 2016. Interpersonal brain synchronization in the right temporo-parietal junction during face-to-face economic exchange. Soc. Cogn. Affect. Neurosci. 11 (1), 23–32. https://doi.org/10.1093/scan/nsv092.

To, C., Kilduff, G.J., Ordoñez, L., Schweitzer, M.E., 2018. Going for it on fourth down: rivalry increases risk taking, physiological arousal, and promotion focus. Acad. Manage. J. 61 (4), 1281–1306. https://doi.org/10.5465/amj.2016.0850.

Tsuzuki, D., Jurcak, V., Singh, A.K., Okamoto, M., Watanabe, E., Dan, I., 2007. Virtual spatial registration of stand-alone fNIRS data to MNI space. NeuroImage 34 (4), 1506–1518. https://doi.org/10.1016/j.neuroimage.2006.10.043.

van Baar, J.M., Halpern, D.J., FeldmanHall, O., 2021. Intolerance of uncertainty modulates brain-to-brain synchrony during politically polarized perception. Proc. Natl. Acad. Sci. U. S. A. 118 (20). https://doi.org/10.1073/pnas.2022491118.

Viscusi, W.K., Phillips, O.R., Kroll, S., 2011. Risky investment decisions: How are individuals influenced by their groups. J. Risk Uncertain. 43 (2), 81–106. https://doi.org/10.1007/s11166-011-9123-3.

Vlaev, I., Chater, N., 2006. Game relativity: How context influences strategic decision making. J. Exp. Psychol. Learn. Mem. Cogn. 32 (1), 131–149. https://doi.org/10.1037/0278-7393.32.1.131.

Wan Lee, S., Shimojo, S., O'Doherty, J.P., 2014. Neural computations underlying arbitration between model-Based and model-free learning. Neuron 81 (3), 687–699. https://doi.org/10.1016/j.neuron.2013.11.028.

Wang, H., Li, L., 2024. Effects of two-person synchronized cycling exercise on interpersonal cooperation: a near-infrared spectroscopy hyperscanning study. Int. J. Clin. Health Psychol. 24 (3), 100492. https://doi.org/10.1016/j.ijchp.2024.100492.

Wang, L., Ayaz, H., Izzetoglu, M., Onaral, B., 2017. Evaluation of light detector surface area for functional Near Infrared Spectroscopy. Comput. Biol. Med. 89, 68–75. https://doi.org/10.1016/j.compbiomed.2017.07.019.

Wang, J.X., Kurth-Nelson, Z., Kumaran, D., Tirumala, D., Soyer, H., Leibo, J.Z., Botvinick, M., 2018. Prefrontal cortex as a meta-reinforcement learning system. Nat. Neurosci. 21 (6), 860–868. https://doi.org/10.1038/s41593-018-0147-8.

Wetzels, R., Vandekerckhove, J., Tuerlinckx, F., Wagenmakers, E.-J., 2010. Bayesian parameter estimation in the expectancy valence model of the Iowa gambling task. J. Math. Psychol. 54 (1), 14–27. https://doi.org/10.1016/j.jmp.2008.12.001.

Worthy, D.A., Maddox, W.T., 2014. A comparison model of reinforcement-learning and win-stay-lose-shift decision-making processes: A tribute to WK Estes. J. Math. Psychol. 59, 41–49. https://doi.org/10.1016/j.jmp.2013.10.001.

Wu, X., Zhu, R., Gong, X., Luo, Y., Liu, C., 2023. Social incentives foster cooperation through guilt aversion: An effect that diminishes with primary psychopathic traits. PsyCh J. 12 (3), 389–398. https://doi.org/10.1002/pchj.641.

Xia, M.R., Wang, J.H., He, Y., 2013. BrainNet Viewer: a network visualization tool for Human Brain connectomics. Plos One 8 (7), e68910. https://doi.org/10.1371/journal.pone.0068910.

Xu, S., Pan, Y., Wang, Y., Spaeth, A.M., Qu, Z., Rao, H., 2016. Real and hypothetical monetary rewards modulate risk taking in the brain. Sci. Rep. 6 (1), 29520. https://doi.org/10.1038/srep29520.

Xue, H., Lu, K., Hao, N., 2018. Cooperation makes two less-creative individuals turn into a highly-creative pair. NeuroImage 172, 527–537. https://doi.org/10.1016/j.neuroimage.2018.02.007.

Yang, J., Zhang, H., Ni, J., de Dreu, Ma, Y., 2020. Within-group synchronization in the prefrontal cortex associates with intergroup conflict. Nat. Neuro. 23 (6), 754–760. https://doi.org/10.1038/s41593-020-0630-x.

Ye, J., Tak, S., Jang, K., Jung, J., Jang, J., 2009. NIRS-SPM: Statistical parametric mapping for near-infrared spectroscopy. NeuroImage 44 (2), 428–447. https://doi.org/10.1016/j.neuroimage.2008.08.036.

Yin, Q., et al., 2025. Uncovering the neural basis of risk preferences in cooperative Dyads: A fNIRS study. NeuroImage 310, 121167. https://doi.org/10.1016/j.neuroimage.2025.121167.

Zanini, L., Picano, C., Spitoni, G.F., 2024. The Iowa gambling Task: Men and Women perform differently. A Meta-analysis. Neuropsychol. Rev. https://doi.org/10.1007/s11065-024-09637-3.

Zhang, R., Liu, J., Li, X., 2019. Neural mechanisms of fairness formation in the perspective of social interactions. Acta Psychologica Sinica 51 (9), 1007–1017. https://doi.org/10.3724/SP.J.1041.2019.01007.

Zhang, M., Jia, H., Zheng, M., Liu, T., 2021. Group decision-making behavior in social dilemmas: Inter-brain synchrony and the predictive role of personality traits. Pers. Individ. Dif. 168, 110315. https://doi.org/10.1016/j.paid.2020.110315.

Zhang, et al., 2023a. Impulsivity-related right superior frontal gyrus as a biomarker of internet gaming disorder. Gen. Psychiatr. 36 (4), e100985. https://doi.org/10.1136/gpsych-2022-100985.

Zhang, W., Qiu, L., Tang, F., Li, H., 2023b. Affective or cognitive interpersonal emotion regulation in couples: an fNIRS hyperscanning study. Cerebral Cortex 33 (12), 7960–7970. https://doi.org/10.1093/cercor/bhad091.

Zhang, W., Qiu, L., Tang, F., Sun, H.-J., 2023c. Gender differences in cognitive and affective interpersonal emotion regulation in couples: an fNIRS hyperscanning. Soc. Cogn. Affect. Neurosci. 18 (1). https://doi.org/10.1093/scan/nsad057.

Zhang, Y., Ye, W., Yin, J., Wu, Q., Huang, Y., Hao, N., Cai, D., 2024. Exploring the role of mutual prediction in inter-brain synchronization during competitive interactions: an fNIRS hyperscanning investigation. Cerebral Cortex 34 (1). https://doi.org/10.1093/cercor/bhad483.

Zhao, H., Li, Y., Wang, X., Kan, Y., Xu, S., Duan, H., 2022. Inter-brain neural mechanism underlying turn-based interaction under acute stress in women: a hyperscanning study using functional near-infrared spectroscopy. Soc. Cogn. Affect. Neurosci. 17 (9), 850–863. https://doi.org/10.1093/scan/nsac005.

Zhao, H., Zhang, C., Tao, R., Duan, H., Xu, S., 2023. Distinct inter-brain synchronization patterns underlying group decision-making under uncertainty with partners in different interpersonal relationships. NeuroImage 272. https://doi.org/10.1016/j.neuroimage.2023.120043.

Zhao, H.X., et al., 2021. Acute stress makes women's group decisions more rational: A functional near-Infrared spectroscopy (fNIRS)-Based hyperscanning study. J. Neurosci. Psychol. Econ. 14 (1), 20–35. https://doi.org/10.1037/npe0000138.

Zheng, L.F., Chen, C.S., Liu, W.D., Long, Y.H., Zhao, H., Bai, X.L., Lu, C.M., 2018. Enhancement of teaching outcome through neural prediction of the students' knowledge state. Human Brain Mapping 39 (7), 3046–3057. https://doi.org/10.1002/hbm.24059.

Zhou, S., et al., 2022. The effect of task performance and partnership on interpersonal brain synchrony during cooperation. Brain Sci 12 (5), 635. https://doi.org/10.3390/brainsci12050635.